January 2017

Investigating Cloud Condensation Nuclei Activity And Particle Growth Of Aging Diesel Exhaust Particles

Humphrey Chigozie Chukwuto

INVESTIGATING CLOUD CONDENSATION NUCLEI ACTIVITY AND PARTICLE GROWTH OF AGING DIESEL EXHAUST PARTICLES

by

Humphrey Chigozie Chukwuto
Bachelor of Engineering, City College of New York, 2013

A Thesis

Submitted to the Graduate Faculty

of the

University of North Dakota

in partial fulfillment of the requirements

for the degree of

Master of Science

Grand Forks, North Dakota, USA

December
2017

This thesis, submitted by Humphrey Chigozie Chukwuto in partial fulfillment of the requirements for the degree of Master of Science in Chemical Engineering from the University of North Dakota, has been read by the Faculty Advisory Committee under whom the work has been performed and is hereby approved.

Dr. Frank Bowman, Chair

Dr. Gautham Krishnamorthy, Committee Member

Dr. Clement Tang, Committee Member

This thesis is being submitted by the appointed advisory committee as having met all of the requirements of the School of Graduate Studies at the University of North Dakota and is hereby approved.

Grant McGimpsey Ph.D.
Dean of the School of Graduate Studies

December 6, 2017
Date

PERMISSION

Title	Investigating Cloud Condensation Nuclei Activity and Particle Growth of Aging Diesel Exhaust Particles
Department	Chemical Engineering
Degree	Master of Science

In presenting this thesis in partial fulfillment of the requirements for a graduate degree from the University of North Dakota, I agree that the library of this University shall make it freely available for inspection. I further agree that permission for extensive copying for scholarly purposes may be granted by the professor who supervised my thesis work or, in his absence, by the Chairperson of the department or the dean of the School of Graduate Studies. It is understood that any copying or publication or other use of this thesis or part thereof for financial gain shall not be allowed without my written permission. It is also understood that due recognition shall be given to me and to the University of North Dakota in any scholarly use which may be made of any material in my thesis.

Humphrey C. Chukwuto
December 7, 2017

TABLE OF CONTENTS

LIST OF FIGURES

LIST OF TABLES

Table Page

ABBREVIATIONS

Abbreviations	Full Meaning
AIM	Aerosol Instrument Manager
BC	Black Carbon
CCN	Cloud Condensation Nuclei
CCNc	Cloud Condensation Nuclei Counter
CPC	Condensation Particle Counter
DMA	Differential Mobility Analyzer
EC	Elemental Carbon
FEP	fluoroethylene propylene
IN	Ice Nuclei
LVOC	Low Volatility Organic Compound
NVOC	Nonvolatile Organic Compounds
OD	outer diameter
OM	Organic Matter
OPC	Optical Particle Counter
PAH	polycyclic aromatic hydrocarbons
PPB	Part Per Billion
PM	Particulate Matter

POA	Primary Organic Aerosols
RH	Relative Humidity
SLPM	Standard Liter Per Minute
SMPS	Scanning Mobility Particle Sizer
SOA	Secondary Organic Aerosol
SS	Supersaturation
SVOC	Semi Volatile Organic Compound
UND	University of North Dakota
UV	Ultra-Violet
VOC	Volatile Organic Compound
WHO	World Health Organization

NOMENCLATURE

a_w	Water activity
C_c	Cunningham slip correction
CCN/CN	Activation ratio
D_m	Particle's mobility diameter
D	Droplet diameter
D_c	Droplet critical diameter
D_p	Particle diameter [µm or nm]
D_{pc}	Critical particle diameter [µm or nm]
Dp^{mean}	Particles' mean diameter
e	Elementary charge
k_w	Particle Wall- loss rate constant
k_{wavg}	Average particle wall- loss rate constant
k_{wlower}	Lower particle wall- loss rate constant
k_{wupper}	Upper particle wall- loss rate constant
L	Length of DMA rod
q_{sh}	Sheath flow rate
M_0	Initial corrected mass at the state of the experiment

M_{end}	Final corrected mass at the end of the experiment
$M_{\alpha\text{-pinene}}$	Molecular weight of α-pinene
M_w	Molecular weight of water
n	Number of elementary charges
n_s	Moles of the solute
n_w	Moles of water
P	Vapor pressure of the cloud droplet
P_0	Saturation pressure of pure water
ρ_w	Density of water
R	Universal gas constant
r_1 and r_2	Inner and outer radius of the DMA
S	Saturation ratio
Sc	Critical supersaturation
S_K	Kelvin ratio or
S_R	Raoult saturation ratio
V	Voltage
V_s	Solute volume
V_T	Total droplet volume
V_w	Water volume
μ	Gas viscosity
T	Absolute temperature
Y	Total Secondary organic aerosol yield

κ	kappa
κ_{CCN}	Cloud Condensation Nuclei based kappa
γ_w	water activity coefficient
χ	Particle's dynamic shape factor
χ_w	Mole fraction of water
σ_{Wo}	Air- water surface tension
ΔHC	Mass concentration α-pinene consumed
ΔM	Change in mass
ΔM%	Percentage change in mass
ΔT	Temperature difference between the top bottom column of CCN counter

ACKNOWLEDGEMENTS

I would like to thank National Science Foundation, North Dakota EPSCoR, SUNRISE Education and Research Program, College of Engineering & Mines, Department of Chemical Engineering and School of Graduate Studies at the University of North Dakota for the financial support and the privilege given to me to pursue my Master of Science in Chemical Engineering in this prestigious institution.

I would like to thank my advisor Dr. Frank Bowman for his help, advice, guidance and encouragement during the entire duration of my master program. I would also like to extend gratitude to my committee members, Dr. Gautham Krishnamoorthy and Dr. Clement Tang for their support and co-operation towards completion of this thesis.

I sincerely thank my colleagues within Dr. Bowman's research group for their tremendous support and help. Special thanks to Richard Cochran, Nicolas LaFosse, Nicole Larson, Ellen Walstad, Alexis Tupy, and Carlos Bucaram for their helps throughout this project.

Finally, I would like to thank my family and friends for their love and support through all my life. Special thanks to my wife Heather Chukwuto and my brother Uzoma Chito for their support and encouragement throughout my academic pursuit.

ABSTRACT

Soot particles are an essential atmospheric constituent because of their effects on human health, regional and global climate. The impact of soot on climate and human health depends on their ability to interact with water vapor. Freshly emitted soot particles are hydrophobic but the chemical and physical transformations (aging) they undergo while airborne can make them hydrophilic enough to retain water and act as nuclei for cloud formation. The aging of soot is a complicated process and represents a significant uncertainty in quantifying the net radiative forcing of soot particles. In this study, the cloud condensation nuclei (CCN) activity and the secondary organic aerosol formation of diesel exhaust aged in the presence of one or more of the following: UV-radiation, α-pinene, and ammonium sulfate seed particles were investigated. Four sets of experiments (diesel exhaust, diesel exhaust + α-pinene, diesel exhaust + ammonium sulfate seed particle, and diesel exhaust + α-pinene + ammonium sulfate seed experiments) were conducted. The changes in size distribution, number concentration and CCN activity of the aged diesel exhaust particles were monitored with Scanning Mobility Particle Sizer (SMPS) and Cloud Condensation Nuclei Counter (CCNc).

Results from dark experiments with diesel exhaust alone reveal no significant secondary organic aerosol (SOA) formation, nor CCN activation for fresh and aged diesel exhaust particles, as indicated by decreases in particle mass with time (mass decreased by a factor of 0.3), near zero kappa ($\kappa_{CCN} \sim 0$) and activation ratio (< 1%) values at all times, and large critical diameters.

Aging of diesel exhaust particles in the presence of UV- radiation in the diesel exhaust experiments resulted in a significant increase in mass (increased by factor of 1.0-1.4), kappa value (ranging from 0.03-0.08), activation ratio (ranging from 0.1-0.75), and a substantial decrease in critical diameter after 200 minutes of aging.

The addition of 39 ppbv of α-pinene (diesel exhaust + α-pinene experiments) further enhanced CCN activation and SOA formation of diesel exhaust particles exposed to UV radiation. K_{CCN} values (0.08-0.15) and particle mass (increased by a factor 1.4 – 1.7) increased further by 88% and 21%, respectively, when compared to the diesel exhaust experiments. Also, the addition of α-pinene reduced the particle diameter required for activation.

Experiments with a mixture of diesel exhaust and ammonium sulfate seed particles under UV and dark conditions investigated the effect on ammonium sulfate seed particles on SOA formation and CCN activation. Over the course of an experiment, particle mass in dark experiments decreased by a factor of 0.9-0.8, while particle mass in the UV experiments increased by a factor of 1.1-1.2. The result shows that SOA formation was higher for diesel exhaust experiments than when a mixture of diesel exhaust and ammonium seed particle were exposed to UV radiation. K_{CCN} of the aged particles, which seems to be correlated with the ammonium sulfate fraction and the % increase in particle mass, was found to range from 0.02-0.3 for UV experiments.

The addition of 39 ppbv of α-pinene to the mixture of diesel exhaust and ammonium sulfate had a significant effect on particle mass (increased by 60%) but no discernible effect on κ_{CCN} when compared to diesel exhaust +ammonium sulfate experiments.

The results from this study underscore the importance of exposure to sunlight (UV), mixing with water-soluble particles, such as ammonium sulfate, and SOA precursors such as gas

phase diesel exhaust and α-pinene, in transforming hydrophobic soot into more CCN-active particles. The increase in hygroscopicity and CCN activity of aged diesel particles is expected to reduce their atmospheric lifetime.

CHAPTER I

INTRODUCTION

1.1 Atmospheric Aerosols

The atmosphere contains particles in size ranging from 0.002 to 100μm (Hinds, 1999, Seinfeld and Pandis, 1998). These airborne solid and liquid particles, called aerosols, have received a lot of attention over the past decades because of their effects on air quality, visibility, human health and climatic conditions. While aerosol is comprised of the particles and their suspending air, the common usage of aerosol refers to the particulate matter (PM). The term aerosol and particulate will be utilized interchangeably in this thesis. The concentration of aerosols in the atmosphere varies with time and space, but the number and mass concentrations of these particles in the troposphere are typically within 10^2-10^5 cm^{-3} and 1-100μgm^{-3} respectively, (Hinds, 1999, and Pöschl, 2005). Once in the atmosphere, the size and composition of aerosol particles are continuously being altered until they are eventually removed from the atmosphere. Depending on their sizes, metrological conditions, and the transformations they undergo in the atmosphere, aerosols typically have an atmospheric lifetime of a few hours to a few weeks (Raes. Et al., 2002, and Williams, et al., 2002).

1.2 Atmospheric Aerosol Classification

The method of classifying aerosols has been a subject of research over the years. Through years of studies, researchers have developed three important methods of classifying atmospheric aerosols. These include classification of aerosols based on their sources, physical properties (size) and chemical composition. The next sections of this paper will explain these three methods of aerosol classification.

1.2.1 Aerosol Sources

Aerosols are emitted into the atmosphere from several natural and anthropogenic sources including mineral dust, volcanic eruptions, sea-salt sprays, natural wild-fires, fossil fuels or bio-fuel combustion processes, man- made wild-fires, changes in land use, and industrial activities (Hinds, 1999, Seinfeld and Pandis, 1998). Primary particles are emitted directly from a wide range of natural and anthropogenic sources, while secondary particles are formed in the atmosphere through the nucleation of gaseous molecules (gas-to-particle conversion) and by condensation of semi-volatile compounds on pre-existing particles (gas-to-particle partitioning).

1.2.2 Aerosol Size Distribution

Particle size (diameter) is the general and most crucial criterion for classifying aerosol behavior. The size of aerosols depends on their source and the mechanism by which they are formed. For example, the diameter (D_p) of a mechanically generated mineral dust particle is an order of magnitude larger than the D_p of a soot particle formed from combustion processes. Atmospheric aerosols are typically divided into two groups, namely fine (D_p<2.5μm) particles and coarse (D_p>2.5 μm) particles (Pandis, and Seinfeld, 1998, Hinds, 1999).

Fine particles are further separated into two different modes, namely, Aitken or nucleation mode particles (~0.01 <D_p< ~0.1μm) and accumulation mode particles (0.1<D_p<2.5μm) (Hinds, 1999, Pandis and Seinfeld, 1998). Fine and coarse particles have a different fate in the atmosphere because they are removed from the atmosphere by different mechanisms. Fine particles are removed mainly by wet deposition (rainout, wash out), while coarse particles are efficiently removed from the atmosphere by gravitational sedimentation or dry deposition

A plot of ambient aerosols' size distribution generally shows three peaks within the size range of 0.01 and 100μm (Hinds.1999, Pandis and Seinfeld, 1998). As shown in Figure 1, the

three peaks separate ambient aerosols into nucleation or Aitken, accumulation, and coarse modes, respectively.

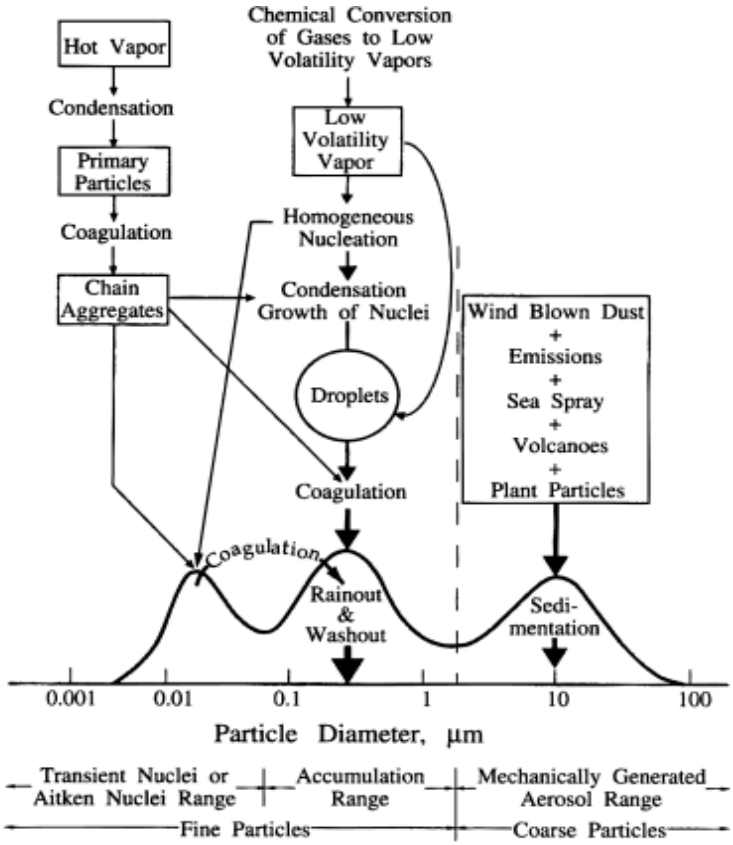

Figure 1. Schematic of an atmospheric aerosol surface area distribution showing the three modes. Figure from Whitby and Cantrell (1976).

Nucleation mode ($D_p < 0.1$ μm) particles are either emitted directly into the atmosphere by combustion processes, (e.g., motor vehicles lead to nucleation mode particles near highways) or are formed by gas-to particle conversion processes in the atmosphere as well as condensation of hot vapors during combustion processes (Hinds, 1998). Due to their high number concentration and relatively small size, particles in nucleation mode coagulate rapidly and end up in accumulation mode.

Accumulation mode particles (0.1 μm < D_p < 2.5 μm) includes particles that have increased in size due to vapor condensation onto existing particles, and coagulated nucleation mode particles (Hinds, 1998). Their relatively long atmospheric lifetime is the reason they are responsible for most aerosol climate effects. Since particles in this mode can act as condensation nuclei for cloud formation, wet deposition remains the efficient mechanism for removing particles in this mode from the atmosphere. (Hinds, 1998).

The coarse mode particles (D_p > 2.5 μm) consist of primary particles emitted into the atmosphere during mechanical processes by natural sources (dust, sea spray), and anthropogenic sources such as agricultural and surface mining activities (Hinds, 1998). Because of their large size, coarse particles readily settle out of the atmosphere shortly after they are emitted.

1.2.3 Aerosol Chemical Composition

The chemical composition of atmospheric aerosols depends on their source and the transformations they undergo while in the atmosphere. The chemical composition of aerosols makes it possible to distinguish aerosols from different sources, e.g., continental aerosols from marine aerosols. Due to the complex transformation of particles in the atmosphere, tropospheric particles are typically composed of both organic and inorganic materials (McFiggans et al., 2006; Middlebrooks et al., 1998).

Aerosols are classified according to their chemical compositions into carbonaceous and inorganic particles (Seinfeld and Pandis 1998). Carbonaceous particles make up a significant fraction of aerosol mass and include particles composed of black carbon (BC) also called elemental carbon (EC) or soot, organic carbon and inorganic carbonate compounds (Tritscher et al.,

2011). BC and EC refer to the same type of material but are used in different contexts. In atmospheric aerosol measurement, the term BC is used when the optical property of soot is being measured, while EC is used when the thermal property is being measured.

Typically, atmospheric particles contain mixtures of different chemical components. The aerosol mixing state describes how chemical components of aerosols are distributed. It classifies aerosols into internally and externally mixed. Aerosols are said to be externally mixed if individual particles consist of a single chemical species and internally mixed when all particles are of mixed chemical composition (Winkler, 1973).

1.2.3.1 Organic Aerosol. Organic aerosols are composed of organic compounds such as n-alkanes, n-alkenes, aliphatic, dicarboxylic acid fatty acids, etc. (Finlayson-Pitts, and Pitts., 2000; Jacobson et al., 2000). They are either directly emitted into the atmosphere (primary organic aerosols, POA), or formed in the atmosphere (secondary organic aerosols, SOA). Sources of POA include forest fires, domestic heating, fossil-fuel combustion (domestic, industrial, traffic), and biomass combustion, etc. (Pöschl, 2005). SOAs are formed in the atmosphere by three different pathways outlined by (Pöschl, 2005).

1. Nucleation and growth of new aerosol particles from semi-volatile organic compounds (SVOCs).
2. Adsorption or absorption of SVOCs in the gas phase on preexisting aerosol or cloud particle or gas-to-particle partitioning.
3. Formation of low volatility or nonvolatile organic compounds (LVOCs, NVOCs) by the chemical reactions of VOCs or SVOCs at the surface or in the bulk of aerosol or cloud particles.

Because of the complexity of organic aerosols found in the atmosphere, it is often difficult to identify organic aerosols as either from primary or secondary sources (Seinfeld and Pandis, 1998; Finlayson-Pitts and Pitts; 2000; Jacobson et al., 2000).

1.2.3.2 Inorganic Aerosol. Atmospheric inorganic aerosols originate from primary particles emitted into the atmosphere and the secondary particles formed in the atmosphere. Inorganic aerosols are dominated by sulfate and nitrate aerosols, except for marine aerosols which are dominated by sodium chloride aerosols (NaCl) (Pöschl, 2005). Primary sources of inorganic aerosols include mineral dusts and sea salt particles.

Secondary inorganic aerosols occur mainly in the form of ammonium sulfate ($(NH_4)_2SO4$ and ammonium nitrate ($(NH_4)_2NO_3$) (Seinfeld and Pandis, 1998). They are formed when ammonia neutralizes sulfuric acid (H_2SO_4) and nitric acid (HNO_3) to form ($(NH_4)_2SO_4$), ($(NH_4)_2NO_3$) respectively (Stockwell et al., 2003). Because of the acidic strength of sulfuric acid relative to nitric acid, ammonia will readily neutralize sulfuric acid over nitric acid when both acids are present in the atmosphere (Seinfeld and Pandis, 1998). The formation of secondary sulfate and nitrate particles strongly depends on several chemical and micro-meteorological factors, like the level of gaseous precursors, the concentration of atmospheric oxidants, the characteristics of preexisting aerosols and the air temperature and humidity (Pathak et al., 2009, Baek et al.,2004). Because the uptake of sulfuric acid is diffusion-limited (Bassett and Seinfeld, 1984), and because the sulfur content of the Earth's crust is too low to be a significant source of primary sulfates, sulfate particles are predominantly in the submicron size range (Pöschl,2005). Nitrate- containing particles tend to take over super-micron range due to the weakness of nitric acid and the volatility of nitric acid, which make it relatively easy for nitric acid to condense on coarse particles (Bassett and Seinfeld, 1984, Pöschl, 2005).

1.3 Aerosol Health Effects

There is growing concern over the health effects of air pollution (Sydbom et al., 2001). Several epidemiological studies show that particulate matter air pollution is linked to severe health issues which include: asthma, chronic bronchitis, respiratory tract infections, cardiovascular diseases, and allergies. (Salvi and Holgate, 1999, Bernstein et al., 2004, Katsouyanni, et al., 2001, Pope et al., 2004, Pope and Dockery, 2009).

Although the human respiratory system is equipped with adequate defense mechanisms (e.g., mucociliary clearance) to deal with particles depositing on its surface, the defense mechanisms could be overwhelmed when the particles accumulating on it are either toxic or high in number (Salvi and Holgate, 1999). The health implications of PM depend on the particle size, structure, solubility, chemical composition, mass, and number concentration (Pöschl, 2005). Figure 2 shows positions where particles of different sizes deposit along the human respiratory system. Large particles with diameters 3 -5µm deposit on the trachea, where they are propelled upward by the mucociliary clearance mechanism into the throat and subsequently swallowed (Salvi and Holgate, 1999). Small particles between 0.1 to 1µm are capable of penetrating through bronchioles into the alveoli where macrophages remove them.

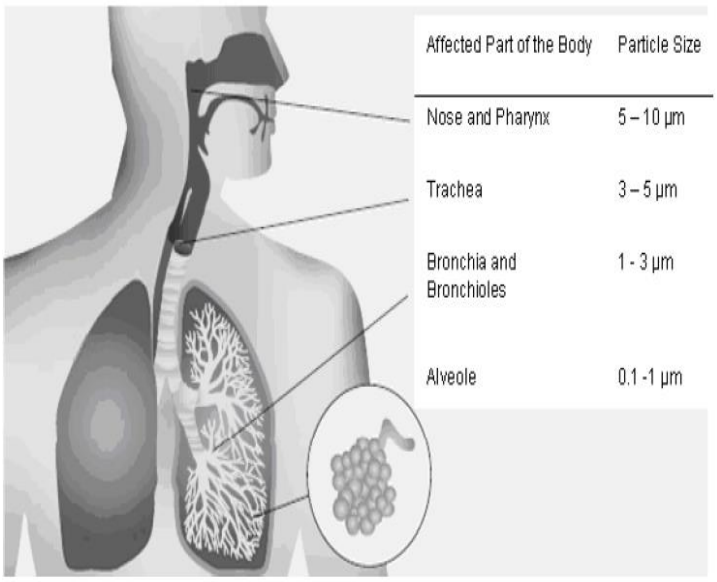

Figure 2 : Respiratory tract and deposition position of different particle sizes. Figure taken from BUWAL (2005).

Besides particle size, the chemical compositions of the particles also determine their health effects. For example, particles composed of transition metals can be redox active. They can generate a reactive hydroxyl radical, which can damage the mucous membrane and cause tissue inflammation (Salvi and Holgate, 1999).

Historically, a high ambient PM concentration has led to three major air pollution episodes. The London smog of 1952 is perhaps the most severe of them. Temperature inversion experienced in the city during a cold December period trapped sulfur emitted from coal fire plants below the ground, thus resulting in a thick fog. The smog mixed with other pollutants and particulate matter (PM) from vehicles to pollute the city air. This tragic event caused over 4000 deaths. A similar pollution episode occurred in Belgium's Meuse Valley in 1930, resulting in about 20 deaths. The city of Donora, Pennsylvania witnessed a smog pollution caused by high ambient PM concentration in 1948. Over 14,000 people became ill, and 20 died.

1.4 Aerosol Effects on Climate and Visibility

Aerosols directly or indirectly exert significant influence on Earth's climate. Aerosols affect the climate due to their ability to scatter, absorb radiation, and serve as nuclei for cloud formation. They also affect air quality by reducing visibility. A particle-free atmosphere has a visibility of approximately 296km at sea level (Seinfeld and Pandis, 2006). Aerosols reduce visibility in the atmosphere to less than a few kilometers due to their ability to scatter and absorb radiation from sunlight (Seinfeld and Pandis, 2006).

1.4.1 Aerosol Direct Effect

Aerosols directly affect Earth's climate by scattering incoming solar radiation and absorbing out-going terrestrial radiation (Haywood and Boucher, 2000, McCormick and Ludwig 1967). The extent of this effect depends strongly on the particle size, composition, concentration, and hygroscopicity. White aerosols such as ammonium sulfate cool the atmosphere by scattering sunlight back to space, while black aerosols like soot warm the atmosphere by absorbing incoming sunlight and outgoing terrestrial radiation. Figure 3 shows the effect aerosols have on the warming and cooling of climate (radiative forcing). Radiative forcing is a measure of the influence greenhouse gasses and aerosols have on the balance of incoming and outgoing energy on Earth's system, and it is measured in Watts per meter squared (W m^{-2}). Negative and positive values of W m^{-2} indicate cooling and warming effects respectively. As shown in Figure 3, an aerosol net direct impact on climate is cooling because aerosol number concentration in the atmosphere is dominated by sub-micrometer particles that can efficiently scatter sunlight back to space (Chin et al., 2009). The error bars in Figure 3 indicates the level of uncertainty surrounding the effect of greenhouse gases and aerosols on climate. It is clear from the error bar that there is less confidence in quantifying aerosols' direct and indirect influence and that more studies are required to improve our quantitative understanding of aerosols' direct and indirect effects.

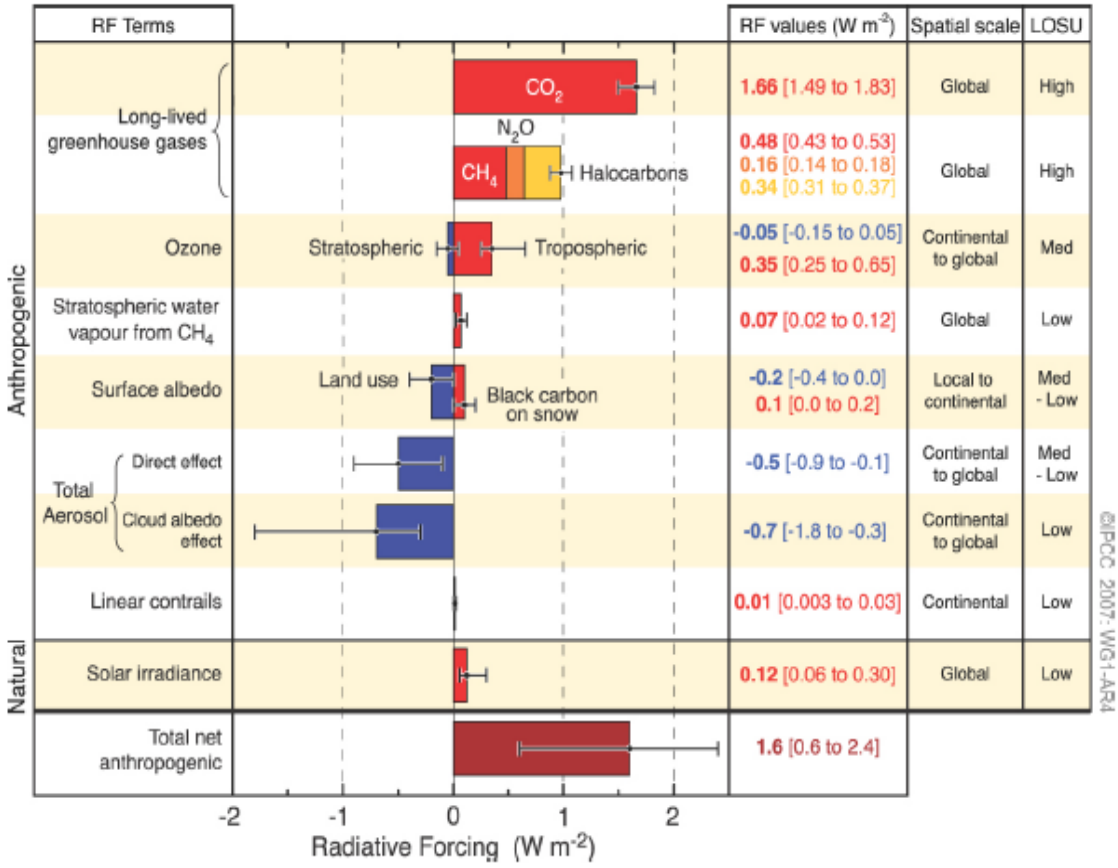

Figure 3. Radiative forcing for principal emissions from preindustrial to 2005. The negative radiative forcing indicates cooling effect while positive radiative forcing indicates warming effect. The error bars indicate uncertainty in representing radiative forcing of each emission (IPCC, 2007)

1.4.2 Aerosol Indirect Effect

Aerosols' indirect effect on climate depends on their ability to act as cloud condensation nuclei (CCN) or ice nuclei (IN) (McFiggans et al., 2006, Seinfeld and Pandis, 1998, Pruppacher and Klett. 2004). By become a CCN, aerosols alter cloud properties such as size, number concentration, cloud albedo, and lifetime (Albrecht, 1989, Twomey, 1974, Warner, 1968).

The roles of aerosol in altering cloud albedo is shown in Figure 4. The upper left of the figure labeled "clean'' shows an unpolluted atmosphere. As can be seen, atmosphere with fewer

particles reflects less radiation from the sun due to a smaller number and larger size of cloud droplets. The figure labeled "polluted" shows more reflection of radiation due to additional particles in the polluted atmosphere acting as CCN. Activation of more particles at fixed atmospheric supersaturation (SS) increases cloud number concentration and cloud albedo, resulting in less radiation from the sun reaching the Earth's surface (climate cooling effect or Twomey effect) (Twomey, 1977). Activation of more particles means more particles competing for the available water vapor and formation of smaller size cloud droplets which tends to reduce precipitation and increase cloud lifetime. The atmospheric cooling effect due to the formation of smaller cloud size is also known as the Albrecht effect (Albrecht, 1989).

The effects of aerosols on climate and clouds depends not only on the number of particles, but also on their chemical composition. Soot particles (lower diagram of Figure 4) incorporated into an existing cloud increase evaporation of the cloud. This process is also known as the semi-direct effect of aerosol reduces cloud lifetime and induces local warming of the atmosphere (Lohmann and Feitcher, 2004).

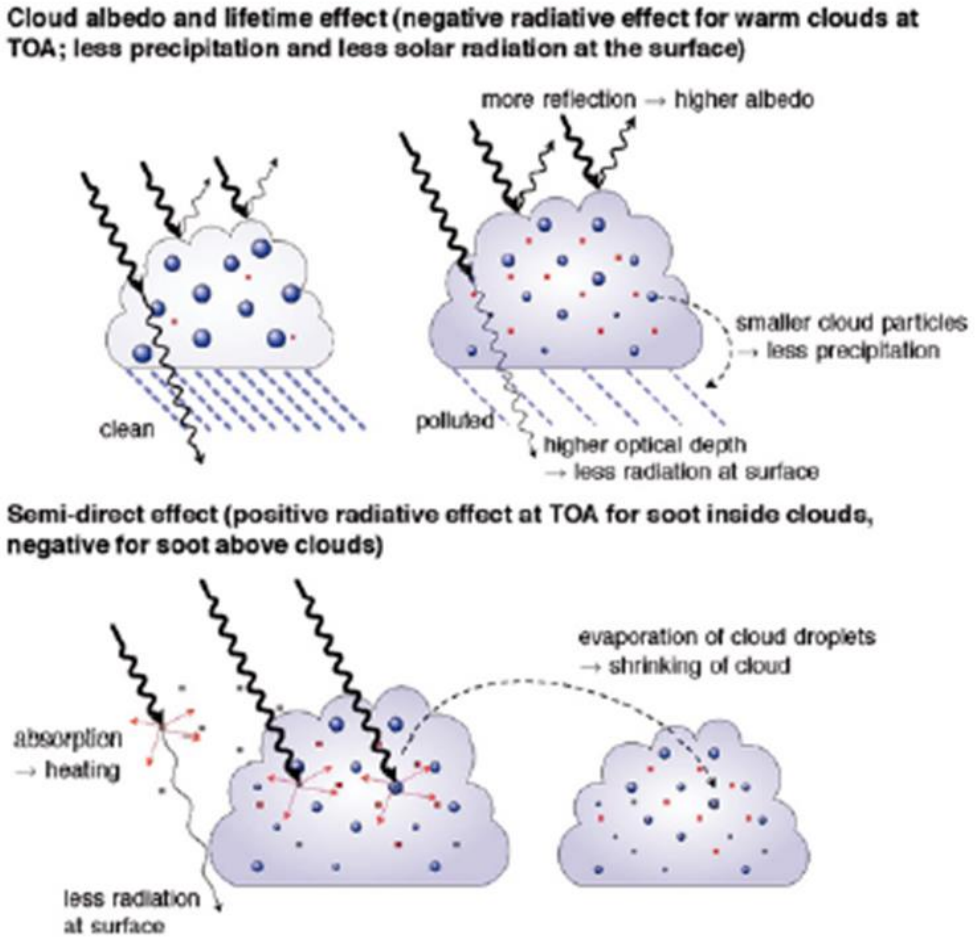

Figure 4 . Diagram of aerosol indirect effect, cloud albedo, cloud lifetime and semi-direct effect at the top-of-the –atmosphere (TOA) (IPCC, 2007)

1.5 Thesis Motivation

The uncertainty in predicting future changes in global climatic conditions can mainly be attributed to incomplete knowledge of atmospheric aerosols' direct and indirect effects. To correctly predict future changes in global climatic conditions, it is imperative to incorporate aerosols' direct and indirect effects into future climate models. To accurately predict aerosol behavior, it is necessary to understand how their properties change over time within the atmosphere.

Diesel particles are emitted into the atmosphere due to incomplete combustion of diesel fuel. Like any other aerosol particles, diesel particles affect global and regional climates and pose

some health risks. While in the atmosphere, they interact with other atmospheric species resulting in significant changes in their physical and chemical properties, CCN activity, and their influence on climate and human health. Their influence on climate and human health can only be understood by characterizing their transformations (aging) in the atmosphere. Since their aging directly impacts their hygroscopicity and CCN activity, a convenient way to monitor aging of diesel particles with different chemical species will be to measure changes in the particles' size and CCN activity, which is the focus of this paper.

Previous studies conducted on diesel particles' aging had focused on characterizing the CCN activities of monodisperse diesel aerosol. In this study, changes in particle size distribution and CCN activity of poly-disperse diesel particles aged in the presence of UV radiation, ammonium sulfate particles, and alpha-pinene vapor were monitored with a scanning mobility particle sizer (SMPS) and cloud condensation nuclei counter.

This work sheds some light on hygroscopicity and CCN activity of fresh and aged diesel particles and compares the hygroscopic parameter (kappa) of diesel particles aged with other chemical species as reported in the literature. It improves fundamental understanding of diesel particles' atmospheric transformation and may also contribute to better future climate models.

Overall, this work tests the hypothesis that aging of fresh diesel exhaust in the presence of UV radiation, ammonium sulfate particles, or alpha-pinene vapor will result in particle growth and enhanced CCN activity of diesel particles with time.

1.6 Thesis Outline

Chapter 1 introduces aerosols background information. It outlines aerosol sources and their effects on climate and human health. In Chapter 2, a comprehensive review of literature on diesel particle aging is presented. It outlines the different pathways of aging aerosols and discusses the interaction between diesel particles and water vapor. Chapter 3 presents a complete

report on the experimental setup, instrumentation, adapted for this work. Chapter 4 presents the data analysis method used and provides typical results as examples of common behavior in the experiments conducted. Chapter 5 discusses in detail results obtained from the experiments conducted for this work. Chapter 6 presents conclusions drawn based on results obtained for this work, followed by recommendations for future work.

CHAPTER II

LITERATURE REVIEW

The quest to fully understand the health and climate effects of soot particles has opened research opportunities focused on studying the atmospheric transformation (aging) of soot particles while airborne. Though the aging process of soot particles is a complicated process due to thousands of species that could be found in the atmosphere, researchers have developed a method of studying this process by just mixing soot particles with a compound (coating) in a smog chamber. Many studies have characterized soot-aging process by measuring changes in their size, mass, hygroscopicity, morphology, optical properties and CCN ability with an appropriate instrument. This chapter presents an overview of previous research studies on soot aging that will serve as a foundation for this thesis. It takes a holistic look at the atmospheric importance of soot particles, the atmospheric transformation of soot particles, aerosols water interaction, and theories governing hygroscopic and CCN ability of aerosol. This chapter also discusses the studies conducted on the coating of soot particle with organic and inorganic compounds, coagulation of soot with inorganic salt particles and their impact on hygroscopicity, CCN ability, and morphology of soot particles**.**

2.1 Importance of Diesel Particles

Soot particles produced by incomplete combustion of fossil fuel, biomass, biofuel, and wood burning are ubiquitous in the troposphere. Fresh soot consists of chainlike aggregates of

spherical primary particles with elemental carbon (EC) or black carbon (BC) as the major component (Seinfeld and Pandis, 2006). Diesel soot contain a mixture of solid BC, organic matter (OM), sulfate, ash, and other components (Kittelson, 1998). They are emitted at an estimated rate of estimated 8-24 Tg yr^{-1} (Penner et al., 1998; Cooke and Wilson, 1996; Liousse et al., 1996), and constitutes about 10-50% of total tropospheric particulate matter (Lary and Toumi, 1999; IPCC, 2007; Penner et al., 1993 Chameides and Bergin, 2002).

Soot has been a subject of many studies in the recent time because they represent a significant fraction of the tropospheric particulate matter (PM) and have a significant influence human health, regional and global climate. Diesel exhaust particles have been linked with several adverse health effects ranging from mutagenicity to overt toxicity (Sydbom et al., 2001). The BC contained in soot can potentially cause adverse health effects including acute, chronic and carcinogenic exposure-related health effect (Koelmans et al., 2006; Pope and Dockery 2006). According to the World Health Organization (WHO, 2012), exposure to diesel emission is carcinogenic. Besides their health effects, they also have a significant impact on global and regional climate through aerosol direct and indirect effects. The direct effect of soot on climate is due to the ability of BC often found in them to absorb light over a broad range of the solar spectrum (Guo et al., 2016). BC contributes significantly to climate change by direct forcing (Foster et al., 2007) and has been classified as the second largest contributor to global warming after carbon dioxide (CO_2) (IPCC,2007; Jacobson, 2001). The presence of soot in atmosphere, reduces visibility,

modifies near surface photochemical activity, tropospheric ozone production (Li et al., 2005; Lei et al ,2004), and stabilizes the atmosphere by cooling of the surface and heating the atmosphere, which decreases cloud formation, convective strength and precipitation (Fan et al., 2008). In addition to their direct effects on climate, they also indirectly affect climate and air quality by modifying cloud formation and cloud albedo. The indirect effect of soot depends on their source and the transformation (aging) they undergo while being transported in the atmosphere. Currently, the direct and indirect forcing due to soot particles represents large uncertainty in climate prediction (Foster et al., 2007) due to the complex transformation they undergo while the atmosphere.

2.2 Atmospheric Transformation of Soot Particles

Freshly emitted diesel particles are hydrophobic and absorb a significant amount of light due to their high BC content. Once emitted into the atmosphere, they transform (aging) when exposed to water vapor, gaseous species, and other particles in the atmosphere. This atmospheric transformation changes their physical, and chemical properties enhance their CCN activity and their impacts on air quality, climate forcing, and human health (Qiu et al., 2012). The aging of soot is a complicated process and may occur through different mechanisms. Weingartner et al., (1996), outlined the possible mechanisms or pathways by which soot particles age in the atmosphere. These paths include

1. Coagulation of soot particles with other soluble aerosols like ammonium sulfate aerosols (discussed further in section 2.6).
2. Photochemical oxidation on soot particles by UV radiation (section 2.7).
3. The condensing a soluble gaseous component, for example, VOC on the particle surface (section 2.8).

4. Cloud processing (incorporating the particle into existing cloud). Cloud processing of soot particle will not be discussed further in this thesis because this study is focused on the first three aging mechanisms.

Furthermore, aging of soot not only modify their physical and chemical properties but may also enable a hydrophobic soot particle to interact with water vapor and eventually act as CCN. The ability of aged soot particles to interact with water vapor is essential in understanding their atmospheric residence time, the deposition process and their impact on climate, tropospheric chemistry and human health (Zuberi et al., 2005). Laboratory studies conducted have shown that aged soot attracts and retain water. The ability of aged soot particles to retain water and activate into cloud droplets remain their efficient removal process (Zuberi et al., 2005). Before discussing those studies conducted on the first three soot aging pathways, it will be vital to examine how aerosols (soot) interact with water and ultimately act as CCN.

2.3 Cloud Formation and Aerosol Water Interaction

Water exists in the atmosphere as water vapor and liquid droplet. The amount of water in the atmosphere is controlled by the rate of evaporation and sublimation from the Earth's surface, its transport in the atmosphere, and the amount that is removed by precipitation (Pruppacher and Klett, 1978). The interaction between aerosols and water vapor constitutes the essential atmospheric transformation of aerosols. Water vapor condenses preferentially on CCN particles causing them to increase in size and eventually activate into a cloud droplet when the prevailing relative humidity in the atmosphere exceeds 100%.

The process of cloud formation occurs either by homogeneous or heterogeneous nucleation. Homogeneous nucleation or self- nucleation involves condensation of water vapor into cloud droplet without a condensation nucleus. Homogeneous nucleation requires the condensed

water droplet coagulating or sticking together form a 10μm cloud droplet. Cloud formation hardly occurs through homogeneous nucleation due to difficulty in attaining the relative humidity (800%) required for homogenous nucleation (Seinfeld and Pandis, 1998). Since atmospheric supersaturation (SS) hardly exceed 2% (Seinfeld and Pandis, 1998; Pruppacher and Klett, 1978), heterogeneous nucleation (condensation by which aerosols act as condensation nuclei) remains the cloud formation mechanism in the atmosphere. The presence of condensation nuclei reduces the relative humidity (RH) required to form a cloud so that clouds are formed at a RH slightly above 100%. The fraction of the aerosol population that act as condensation nuclei during cloud and ice are formation are referred to as cloud condensation nuclei (CCN) and ice nuclei(IN) respectively. The ability of a particle to act as a CCN depends largely on the particle size, its solubility, wettable of the particles, and the prevailing atmospheric relative humidity (RH) in the atmosphere. A large particle is more likely to act as CCN than small particle if they have the same chemical composition.

2.4 Köhler Theory

As the atmosphere strives to establish equilibrium between its liquid and gas phase water, water vapor in the atmosphere condenses on CCN particles to form a cloud. Unlike equilibrium involving a flat liquid surface, this phase equilibrium is complicated by droplet curvature and by the solubility of the CCN particle involved in cloud formation (Seinfeld and Pandis, 1998). Köhler theory (Kohler, 1936) was the first theory to describe equilibrium between water vapor and liquid droplet in the atmosphere. The theory comprises of curvature or Kelvin effect of the droplet and solubility or Raoult effect of the CCN particles. An overview of Köhler theory and the derivation of Köhler equation presented in this thesis will be based on Hinds (1999), and Seinfeld, and Pandis (1998) if no other reference is mentioned.

Kelvin effect describes how vapor pressure of a curved surface liquid (example cloud droplet) depends on the diameter of the curvature. If a flat surface liquid is at equilibrium with its vapor phase, the vapor pressure over the liquid phase is always equal to its saturation vapor pressure. However, when the surface of the liquid is slightly curved, the vapor pressure over the liquid phase will be greater than that of a flat liquid surface (Hinds. 1999) due to the additional Gibbs free energy required to form the curvature. Also, the curvature of the liquid reduces the net inward attractive force of the liquid phase, thereby making it increasingly easier for water molecules to leave the droplet surface to the vapor phase (Curry and Webster, 1999, Hinds, 1999, Seinfeld and Pandis, 1998). Since water molecules evaporate faster from curved surface relative to a flat surface, the vapor pressure over a curved surface will always be greater than that of flat surface liquid. Kelvin equation (Equation 2.1) shows the relationship between equilibrium saturation pressure of a curved droplet and the droplet diameter. It is derived from the difference between Gibbs free energy of flat and curved surface water at equilibrium with their respective vapor:

$$\frac{P}{P_0} = S_k = \exp\left(\frac{4\sigma_{wo}M_W}{RT\rho_w D}\right) \qquad 2.1$$

where P is the vapor pressure above the droplet, P_0 the saturation vapor pressure of flat surface water at same temperature as the droplet. Σ_{Wo} is the air- water surface tension, $M_w$is the molecular weight of water, ρ_w is density of water, T is the absolute temperature of the droplet, R is the universal gas constant, S_K is the Kelvin ratio or saturation ratio for Kelvin effect, and D is the diameter of the droplet.

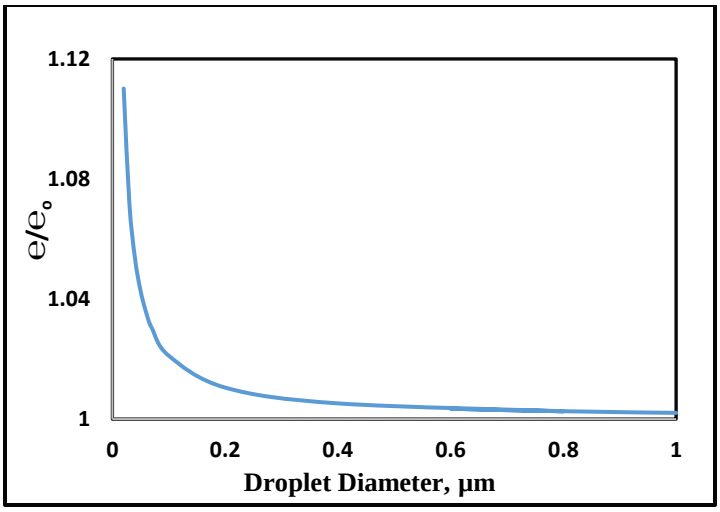

Figure 5. Kelvin effect or the dependence of equilibrium vapor pressure on droplet diameter.

From Figure 5, saturation pressure of a curved surface liquid depends strongly on the diameter of the curvature. A high vapor pressure is required to maintain equilibrium for smaller droplet due to the high rate of evaporation. As the droplet diameter increases, the rate of evaporation decreases and the vapor pressure over the curved liquid approaches vapor pressure of a flat liquid. Also, for a given droplet diameter, there is only one S_k at which the droplet is stable. The droplet will grow if vapor pressure in the atmosphere exceeds S_K and evaporates when it is less (Hinds, 1999).

Raoult or solubility effect is the second competing effect in Köhler theory. It describes how CCN particles lower equilibrium vapor pressure over a droplet. When solute such as Sodium chloride (NaCl) dissolves in water, it lowers water's vapor and prevent water molecules from evaporating. Since less water molecules evaporates, the equilibrium vapor pressure over the aqueous solution is lowered. CCN particles have similar effect when they dissolve in the atmosphere to form a liquid droplet. They lower vapor pressure over droplet and allow the droplet to grow into cloud droplet at a relative low SS.

$$\frac{P}{P_0} = S_R = {}^{\chi}{}_w \gamma_w = a_w \qquad \text{Non-ideal solution} \qquad 2.2$$

where P is vapor pressure over the solution, P_o is the vapor pressure over pure water, ${}^{\chi}{}_w$ is mole fraction of water, γ_w is the activity coefficient of water, a_w is water activity and S_R is Raoult saturation ratio. For highly diluted solution, $\gamma_w \rightarrow 1$ and equation 2.2 reduces to

$$\frac{P}{P_0} = S_R = {}^{\chi}{}_w \qquad \text{Raoult's law} \qquad 2.3$$

The water mole fraction is given below

$${}^{\chi}{}_w = \frac{n_w}{n_w + n_s} \qquad 2.4$$

Where n_w is the number of moles of water, and n_s is of moles of the solute. Since the mole fraction of water in equation 2.4 will be less than one, the solute reduces equilibrium vapor pressure over the droplet solution (Seinfeld and Pandis, 1998). A more soluble NaCl and $(NH_4)_2SO_4$ particles are more like to form a cloud droplet than slightly soluble organic particle because of their ability to significantly lower SS required for their activation.

Köhler equation incorporates the two competing effects and relates equilibrium vapor pressure over a cloud droplet to the droplet diameter. Kelvin effect increases equilibrium vapor pressure while Raoult's effect decrease equilibrium vapor pressure over a droplet. For non- ideal situation, Köhler equation is given by equation 2.5.

$$\frac{p}{p_0} = S = a_w \exp\left(\frac{4\sigma_{wo} M_w}{RT\rho_W D}\right) \qquad 2.5$$

where S is the saturation ratio. For a dilute solution, Köhler equation simplifies to:

$$\ln\left(\frac{P}{P_0}\right) = \frac{4\sigma_w M_w}{RT\rho_W D} - \frac{6n_s M_w}{\pi\rho_w D^3} \qquad 2.6$$

The first term on the right side of equation 2.6 represents the Kelvin effect while the second term is the Raoult effect. The equation can be simplified further by grouping the constants in each term of equation 2.6 (Seinfeld and Pandis, 1998).

$$\mathrm{Ln}\left(\frac{e}{e_0}\right) = \frac{A}{D_P} - \frac{B}{D_p^3} \qquad 2.7$$

where

$$A = \frac{4\sigma_w M_w}{RT\rho_W} \text{ , and } B = \frac{6n_s M_w}{\pi\rho_w}$$

Köhler theory is best described by plotting the saturation vapor pressure ratio ($\frac{P}{P_0}$, in equation 2.7) as a function droplet size. As shown in Figure 6, (ascending portion, blue curve) the vapor pressure over the droplet is less than the saturation pressure of a pure water due to the dominance of Raoult's effect which depends on cube inverse of the droplet diameter (equation 2.7). As the droplet increases, SS increase due to the relative importance of Kelvin effect over the Raoult's effect (Seinfeld and Pandis, 1998). The SS passes through a maximum known as critical supersaturation (S_c) and begin to approach 0 % as the droplet grow into a cloud droplet. For every S_c, there is a certain droplet size or critical diameter (D_c) that can act can activate. A particle will remain a haze particle (ascending blue line) if SS in the atmosphere is less than it's S_c, but activates to cloud droplet if SS in the atmosphere exceeds the droplet's S_c (descending blue line). Köhler curve explains the different droplet processes occurring the atmosphere. The droplets on the ascending portion of the blue curve are stable. They constantly experience evaporation and condensation and return to their original droplet size. If $0<SS<S_c$, there are two droplet diameters associated with that SS. The droplet size associated with the curve on the left ($D<D_c$, ascending blue curve) is stable. A perturbation of droplet returns it to its original size.

The D associated with the curve on the right (D>Dc, descending curve) will be unstable. The droplet (D>Dc) grows into a cloud droplet. The other scenario explained in Figure 6, is when SS in the atmosphere is higher Sc. At the point where (SS>Sc) there is no point on the curve associated with this scenario. Every droplet on the Köhler curves regardless of their diameter grows into a cloud droplet.

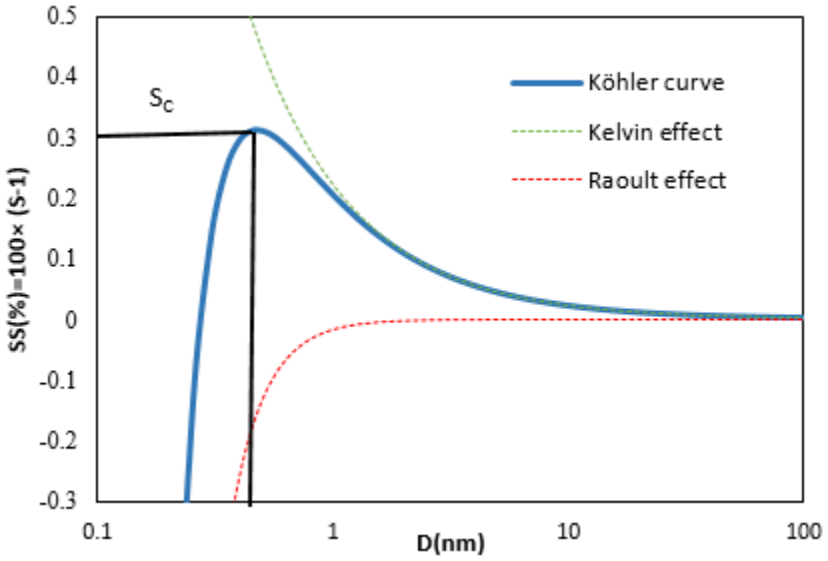

Figure 6. The Köhler Curve. Kelvin effect (green dot line) and Raoult effect (red dot line) The figure was generated for 50nm NaCl diameter particles by assuming that the aerosol particle is spherical, and the mass of solute used in equation 2.7 is obtained by the particle density and volume. T= 298k.

2.5 Hygroscopic and CCN parameter (kappa, κ)

The use of Köhler theory to predict CCN activity of aerosol particles requires knowing the physical and chemical properties of the participating compounds in the particle. Petter and Kreidenweis (2007) developed a single hygroscopicity parameter "kappa (κ)," which doesn't require knowing the physicochemical properties of the participating compounds. Kappa is used to quantify the water uptake characteristics aerosol particle and relate the dry particle diameter to its CNN activity (Petter and Kreidenweis, 2007). The typical kappa values range from 0.5 to 1.4 for

highly soluble inorganic salt particles, 0.01-0.5 for slightly hygroscopic organic particulate matter and zero for non-hygroscopic particles like fresh soot (Petters and Kreidenweis, 2007). Kappa value has a broad range of applications. It predicts particles hygroscopicity growth (particle water content) at relative humidity (RH) <100%, as well as CCN activity insoluble and complex multi-component organic particles at (RH>100%).

The equation relating κ, dry particle diameter, and droplet diameter to saturation vapor pressure over the droplet solution (equation 2.14) derived in this section will be based on (Petter and Kreidenweis,2007) if no other references are mentioned. Kappa is defined in by the parameterization of the water activity, a_w,

$$\frac{1}{a_w} = 1 + \frac{\kappa V_s}{V_w} \qquad 2.10$$

where Vs, Vw are the solute, and water volumes respectively. Assuming Zdanovskii-Stokes and Robison mixing rule, (Stokes and Robinson, 1996) applies, the total droplet volume (V_T) becomes the sum of individual solutes and the water volumes (equation 2.11).

$$V_T = V_W + V_S \qquad 2.11$$

V_T and Vs can be converted to their respective equivalent diameters as follows

$$V_T = \frac{D^3\pi}{6} \qquad 2.12$$

$$V_s = \frac{D_o^3\pi}{6} \qquad 2.13$$

where D is the diameter of the droplet, D_p the dry particle diameter

When equations 2.10-2.13 are combined, α_w is determined. Substituting a_w in equation 2.5 gives the relationship between saturation ratio (S) and particle diameter.

$$S = \frac{D^3 - D_p^3}{(D^3 - D_p^3)(1-\kappa)} \exp\left(\frac{\sigma_s M_w}{RT\rho_w D}\right) \quad 2.14$$

2.6 Coagulation of Soot with Soluble Atmospheric Species

Soluble inorganic particles for example $(NH_4)_2SO_4$ are ubiquitous in the atmosphere. They are either emitted directly or formed in the atmosphere. Coagulation of soot particles with $(NH_4)_2SO_4$ particles may result in larger internally mixed particles that contain both insoluble soot and soluble ammonium sulfate. The mixed particles take up water vapor and get activated into cloud droplet. Transformation of fresh soot to hydrophilic particles via coagulation with soluble inorganic salt particles have been modeled and investigated by some studies.

Kotzick and Niesner (1999) studied the condensation properties of polydisperse of fresh and "benzo[a] pyrene –tagged" soot aged in one of the following: sodium chloride (NaCl), sulfuric acid particles. The critical supersaturation (S_c) (define by the study "as the supersaturation required to activate 50% the particles into cloud droplets") was compared for fresh and aged soot. It discovered that S_c of fresh soot and benzo[a]pyrene-tagged soot was lowered from 25% to 10%. The coagulation of the soot with soluble sodium chloride or sulfuric acid aerosols, reduced Sc from 20 % to 3% after 20 hours.

Fassi et al., (1997) modeled the changes in hygroscopic and optical properties of soot particle from a plume in an environment loaded with accumulation- mode sulfate particles. The model showed that the activation of soot in sulfate particles environment depends on the mixing state, of the particles. However, the study concluded by suggesting that further studies are required to determine the impact of mixing state on hygroscopic property of soot.

Dusek et al., (2006) studied CCN activation of pure and coated carbon black particles generated by nebulizing an aqueous suspension of black carbon. The activation of pure black carbon was found to required higher SS than the SS predicted by Kelvin equation (Kelvin predict SS for insoluble particles). The addition 5%of mass of NaCl to the nebulized aqueous suspension of black significantly enhanced activation of the particles. The SS at which the particles activated was found to agree with the SS predicted by modified Kohler equation (modified Köhler equation predicts SS required by particle consisting of insoluble and coated with a hygroscopic material).

Although coagulation of soot particle with soluble aerosols is one of the atmospheric transformation pathways of soot particles, researchers have focused less on this transformation pathway because they suspect it to be of minor importance (Kotzick and Niesner, 1999) compare to heterogeneous condensation of vapor on soot particle. The few laboratory studies that were conducted, for example, Kotzick and Niesner, (1999) were performed at SS (20% to 3%) that is difficult to attain in the atmosphere. In this thesis, the coagulation as a potential path of transforming hydrophobic diesel exhaust particle to hydrophilic (CCN activity) will be investigated at atmospheric relevant SS (<2%). Also, the particle growth (SOA) of diesel exhaust particle aged in the presence of ammonium sulfate particle will be studied.

2.7 Photochemical Decomposition of Soot Particles

Photochemical decomposition of chemical components on soot surface into more hydrophilic species by O_3 or NO_x or due to UV -radiation is another potential transformation pathway for soot particles (Saxena et al., 1995). For example, the destruction of polycyclic aromatic hydrocarbons (PAH), e.g., benzo[a]pyrene (BaP) located on the soot surface due to incomplete

combustion by UV- radiation (Kotzick and Niesner, 1999). The photochemical decomposition of fresh soot to hydrophilic particles have been investigated by some studies

Kotzick and Niessner (1999) demonstrated the importance of O_3 in transforming a hydrophobic soot particle to the hydrophilic particle. In this study (discussed already in section 2.5), the condensation properties of pure and "benzo[a]pyrene-tagged" soot aged in the presence ozone was investigated. Without ozone, Sc only decreased from 25 to 10% after 20 hours due to the simple coagulation of pure and benzo[a]pyrene-tagged soot. The decomposition of benzo[a]pyrene into polar, hydrophilic products due to the reaction with ozone, however, resulted in significant lowering of S_c from 20 to 2% after 5 hours.

Zuberi et al., (2005) studied the hygroscopic properties of laboratory generated methane and n-hexane soot aged in an extreme oxidizing ($OH/O_3/H_2O/UV$) environment. The experiments conducted in flow tube discovered that no water adsorption or CCN activation of the fresh soot. A reversible water adsorption was observed after aging the soot in an oxidizing environment, and the amount of water adsorbed by the soot particle was a function of relative humidity they (soot particles) were exposed to.

Weingartner et al., (1997) conducted laboratory experiments to investigate the hygroscopic properties of freshly emitted diesel soot particle at sub-saturation (relative humidity <100%). The poly-dispersed fresh diesel particles generated from the diesel engine (Yamaha EDA 4700 T, direct injection, no turbocharger) were reduced to monodisperse particles by a differential mobility analyzer (DMA). Then, the size-selected particles were humidified (RH =95%) and passed to a second DMA and condensation particle counter (CPC) where the size distribution and number concentration of the particles were simultaneously measured. In some experiments, the fresh diesel particles were exposed to ozone before reducing them to monodispersed

particles. It was discovered that fresh diesel particle showed no hygroscopic growth and that the hygroscopicity of the diesel particles was enhanced when sulfur content of the diesel fuel was increase or when the particles were subjected to an ozone and UV pre-treatment.

The photochemical decomposition of chemical components on soot surface into more hydrophilic species by UV will not be independently investigated in this thesis; instead, it will be studied in combination with heterogeneous condensation of vapor discussed in the next section (section 2.8).

2.8 Condensation of Soluble Gaseous Components on Soot Particle Surface

Fresh soot is hydrophobic, but the condensation of more water- soluble organic material can significantly enhance the hygroscopicity and the potential of soot to serve as cloud condensation nuclei (Zhang et al., 2008: Tritscher et al.,2011; Henning, S. et al.2012; Alexei et al.,2009; Hings, et al.,2008; Lambe et al.,2015; Wittbom et al.,2014). It has been shown that changes in the property of soot particles depend on the material condensing on the surface of the particle (Guo et al.,2016). Condensation of water-soluble compounds will enhance CCN activity of soot, while condensation of insoluble material may leave the hygroscopicity and CCN activity of soot unchanged. Some studies have investigated the changes in hygroscopicity and CCN activity of soot coated with different condensable vapor material.

Tritscher et al., (2011) investigated the changes in hygroscopicity of fresh and photochemically aged size selected soot particles from diesel passenger car engine vehicles, EURO3 (with oxidation catalyst) and EURO2 (without oxidation catalyst). They discovered that fresh diesel exhaust particles were unable to undergo hygroscopic growth nor CCN activation. The SOA formed from photooxidation of the VOCs from the diesel exhaust increased the water uptake and CCN activity of the size selected diesel particles.

Qiu et al., (2012) studied the changes in morphology, optical properties and hygroscopicity of monodisperse soot particle exposed to oxidation products from the reaction of OH with toluene. The experiments conducted in 1.2m^3 collapsible environmental chamber monitored the variation in particle size, organic mass fraction, morphology, optical properties and hygroscopicity of the aging soot particle generated from incomplete combustion propane. It was discovered that organic coating of the particles which depends on the reaction time and the initial concentrations of the reactants governed the changes in the properties of soot particles. Increased coating of the particle surface with oxidation products from the reaction of OH with toluene enhanced hygroscopicity of the particles.

Lee et al., (2004) investigated the effect of preexisting diesel soot particle on SOA formation. The study conducted in an outdoor smog chamber under the natural sunlight compared the SOA formation from diesel exhaust to the SOA formation from α-pinene in the presence of preexisting diesel exhaust particles. The study discovered that photochemical reaction of diesel exhaust without α-pinene increased the particle mass by a factor 2 compared to the initial diesel soot particle mass. The addition of 140ppbv of α-pinene increased the mass of the diesel particle by a factor of 4 from the initial diesel soot particle mass. The α-pinene oxidation products analyzed for the gas and particle phase were mostly carbonyl compounds.

Weitkamp et al., (2007) studied the SOA formation from aging diesel exhaust particle under UV radiation. The study discovered a rapid production of SOA during the first hour of photochemical aging of the diesel exhaust. After particle and vapor loss correction, the mass of the aged diesel exhaust doubled its initial mass (58µgm^{-3}). Also, the median diameter of the particles

was observed to increase with the reaction due to the condensation of the semi-volatile compounds on the particle. The study concluded that the ultimate SOA yield was uncertain due the vapor and particle losses in the chamber.

Khalizov et al., (2013), investigated the changes in the physical and chemical properties of size-selected soot particle coated with condensable products from OH and isoprene reaction. This study performed in 1.2m^3 collapsible fluoropolymer chamber monitored the evolution in size, mass, hygroscopicity and CCN activity of the particles. The particle effective density, dynamic shape factor, mass fractal dimension and coating thickness were calculated from the measured particle size and mass. This study discovered that fresh soot exhibited no detectable hygroscopic growth factor at 90% relative humidity and that less than 0.1% of the particle activated into cloud droplets at 1.6% SS. The aging of the particle in the presence of photochemically oxidized isoprene transformed initially hydrophobic soot particle into efficient CCN and promoted restructuring of the coated particles. Also, the increase in mass and diameter were more pronounced for smaller particles than the larger particles.

Nakao et al., (2011) studied the SOA formation from a diluted and undiluted diesel exhaust exposed to UV radiation. This study used the particles' volume calculated from the particle mobility diameter to quantify the SOA formation of the diesel exhaust. It was discovered that the use of volume-based SOA quantification underestimated the SOA formation from diesel exhaust due to the external void space of agglomerate particles. The effective particle densities were observed to be higher for undiluted exhaust particles compared to the diluted exhaust particles. The study suggested the importance of dilution method and the need to evaluate particle mass as opposed to volume when quantifying SOA formation from fractal particle such as diesel exhaust.

Wittbom et al., (2014) studied the CCN activation of diesel exhaust particles and particles from a flame soot generator and VW 1998 Passat vehicle. In this study, diesel exhaust (gas +particles) generated were mixed with a various amount of m-xylene, toluene, and ozone in a $6m^3$ Teflon bag reactor. Before the onset of UV radiation, it was showed that freshly emitted soot particles did not activate into cloud droplets at supersaturations≤2%. An immediate change in cloud-activation properties of the particles was observed at the onset of UV exposure. The study concluded that change of cloud condensation nuclei (CCN) properties of the particle s observed at the onset of UV radiation implies that the lifetime of soot particles in the atmosphere is affected by the access to sunlight.

Zhang et al., (2008) showed that soot particles aged in the presence of sulfuric acid vapor acquire a large mass fraction of sulfuric acid during atmospheric aging and experience a considerably change in their physical and chemical properties. In this study, soot particles generated by incomplete combustion of propane were size selected and exposed to sulfuric acid vapor in a 50cm-long reservoir containing 86-96wt% sulfuric acid. This study discovered that soot particle exposed to sulfuric acid vapor experience the large hygroscopic size and mass growth at 90% relative humidity and act efficiently as CCN. It was also discovered that coating with sulfuric acid and subsequent hygroscopic growth enhance the optical properties of soot aerosols, increasing scattering by approximately 10-fold and absorption by nearly 2-fold at 80% relative humidity relative to fresh particles.

Previous studies discussed in section 2.8 (aging of soot by heterogeneous condensation) have been focused characterizing the CCN activity of a monodisperse (size-selected) particle. The two studies similar to this work (thesis), Weitkamp et al., (2007) and Lee et al., (2004) focused on SOA formation without considering the CCN activity of the polydisperse diesel exhaust

particles. In this thesis, the SOA formation and CCN activity of a polydisperse diesel exhaust particle aged by the combination of the aging mechanisms discussed in sections, 2.6, 2.7 and 2.8 will be studied. α-pinene was used as the gas-phase SOA precursor for this thesis because it is the dominant SOA forming compound of the biogenic monoterpenes in the atmosphere(Geron et al., 2000).

CHAPTER III

EXPERIMENTAL METHOD AND MATERIALS

The validity of experimental results depends largely on its set-up and execution. The set-up used for this study is shown in Figure 7. The main components of the set-up include a temperature controlled aerosol chamber holding an $8m^3$ Teflon reaction bag, air generating system, diesel and ammonium sulfate particle generating systems, gas injection and sampling systems, transfer line to inject diesel engine exhaust, and particle sampling system that consists of a scanning mobility particle sizer (SMPS) and cloud condensation nuclei counter (CCNc) to measure changes in size distribution and CCN activity of the particles respectively.

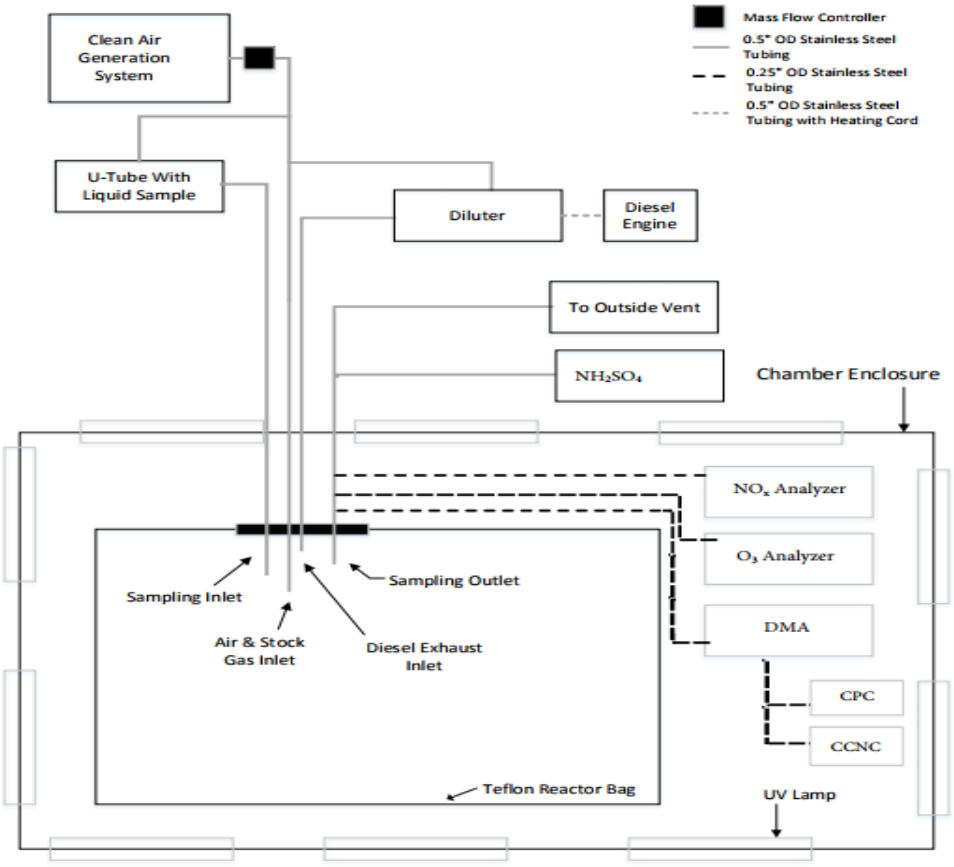

Figure 7. Schematic diagram of University of North Dakota atmospheric aerosol chamber**.**

3.1 Atmospheric Aerosol Chamber

All experiments were conducted in the University of North Dakota (UND) atmospheric aerosol chamber (Figure 8). The chamber consists of an enclosure constructed with fireproof dry-wall panel. To maximize light intensity generated by 81 black lights (40W Sylvania, Danvers, MA), the interior of the chamber is surrounded by a 5-mil (127μm) reflective aluminum sheet

(Nielsen Enterprises, Kent, WA). The chamber enclosure fits an 8 m^3-reactor bag, instrumentation for online gas and particle phase measurements, two space heaters to heat the chamber and two air-conditioning systems to control the chamber's temperature. A desktop computer is placed outside of the chamber to store SMPS data and control flow rate of air and gases injected into the chamber.

Figure 8. Inside of The University of North Dakota (UND) atmospheric chamber enclosure showing UV light fixtures, reflective mirror sheeting and air conditioning units.

3.2 Reactor Bag

The 8m^3 Teflon reactor bag used for this study was constructed by heat sealing 51µm thick 2.35 m x 1.45 m sheets of fluoroethylene propylene (FEP) film (DuPont, Wilmington, DE) with an industrial sealer (West Coast Plastics, Inc., Culver City, CA, USA). FEP was chosen for the reactor because it transmits ultraviolet wavelengths and doesn't readily react with compounds

encountered in this study. The dimension of the reactor (pillow configuration) Figure 9 was selected with the objective of maximizing the reactor's surface area to volume ratio and minimizing the amount of seals required to close the bag. The reactor was supported horizontally by a net stretched approximately 0.1 m off the chamber floor to reduce stress on the reactor. The terms reactor and chamber will be used interchangeably in this paper.

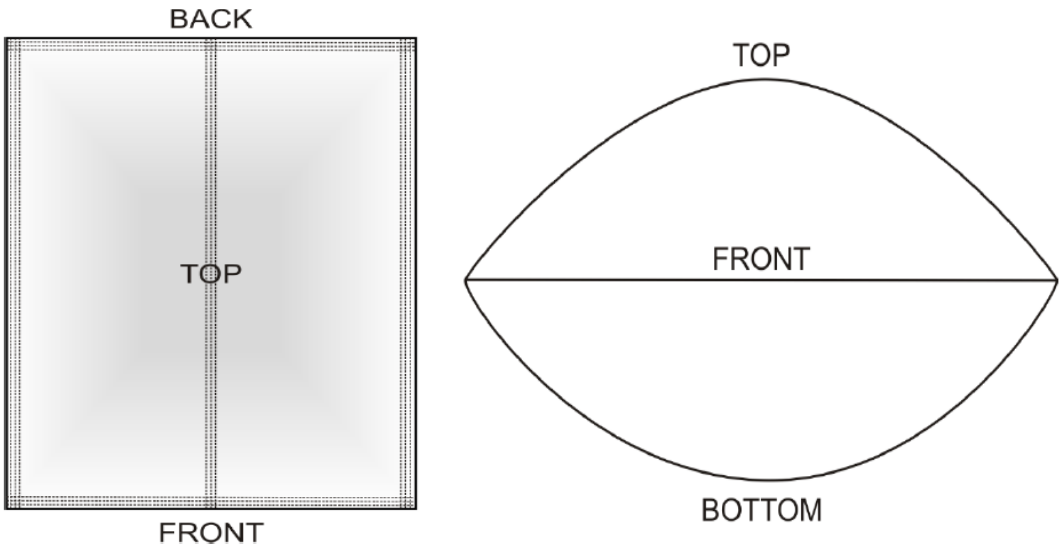

Figure 9. Schematic Diagram of the reactor bag used for CCN activity and particle growth of diesel exhaust Experiments viewed from the top (left) and the front (right).

3.3 Air Generating System

An oil-less air compressor (Hydrovane HVO7, Swindon, Wiltshire UK) connected to a 250-gallon tank supplied air used for this study. The air from the outside was compressed and sent to the tank. The tank served as a reservoir for the large volume of pressurized air required by the pure air generating unit (AADCO 737-14A, Cleves, OH, USA). Before the air was injected into the reactor, the air from the compressor was pre-purified by passing it through two micro-filters (GO5XPDF, GO5ZPDF Parker, Cleve-land, OH, USA) and activated carbon filter

(BAN2L6CUW, Parker). The micro-filters removed dirt, particulates, oils, and water from the air while activated carbon removed gas –phase hydrocarbons. The pre-purified air was dried by passing it through an air refrigeration dryer (Parker Zander ASD25) which removed condensates in the air. The dry air was passed through an additional activated carbon (BAN2L6CUW, Parker) and a pure air generator unit (AADCO 737-14A, Cleves, OH, USA) that reduces the concentrations of gas- phase chemicals (hydrocarbons, ozone, nitrogen oxides) to the values shown in Table 1. Purified air from the pure air generating unit was injected into the reactor at a flow rate of 120SLPM (standard liter per minute) through an injection line made of 0.5″ outer diameter (OD) stainless steel tubing.

Table 1. Concentration of Hydrocarbons and Other Components in the Purified Air.

Chemical Class	Maximum Concentration (ppm)
O_3	< 0.001
SO_2	< 0.001
H_2S	< 0.001
COS	< 0.001
NO_x	< 0.001
CH_4	< 0.005
CO	< 0.005
Hydrocarbons	< 0.005

3.4 Diesel engine

The Diesel exhaust (gaseous components and particles) was generated by an idling (1000rpm) V2403 Kubota diesel engine (Kubota, Torrance, CA, USA) placed outside the chamber. The engine, which has a maximum power output of 49.2 kW, was operated with a standard diesel fuel (sulfur content < 0.0015% by volume) purchased from a local fuel station (Loaf 'N Jug, Grand Forks, ND, USA). Before exhaust injection, the engine was allowed to warm up for

10 minutes at 1100rpm. After 10min, the engine was to return to 1000rpm with no additional load applied during the injection period.

Diesel exhaust from the tailpipe of the engine was introduced into the chamber through a 2m heated transfer line. Before operating the diesel engine, the transfer line was heated to about 160 ^{0} C to minimize condensation of exhaust gases along the walls of the transfer line.

3.5 Ammonium Sulfate Particle Generation

Ammonium sulfate ($(NH_4)_2SO_4$) particles were generated by nebulizing an aqueous solution of $(NH4)_2SO_4$ in a pneumatic atomizer Figure 10 (Aerosol Generator 9200, Bechtel, California, USA). The solution was prepared by mixing 1gram of $(NH_4)_2SO_4$ with one liter of ultra-pure water. After the solution was prepared, it was poured into the atomizer solution bottle (see Figure 10). The solution flew through a spray chamber, where it became atomized into droplets by a high velocity compressed air supplied to the spray chamber at 30 psi. The droplets generated passed through a dryer where the solvent was removed by silica gel to generate dry $(NH_4)_2SO_4$ particles injected into the chamber through an injection line.

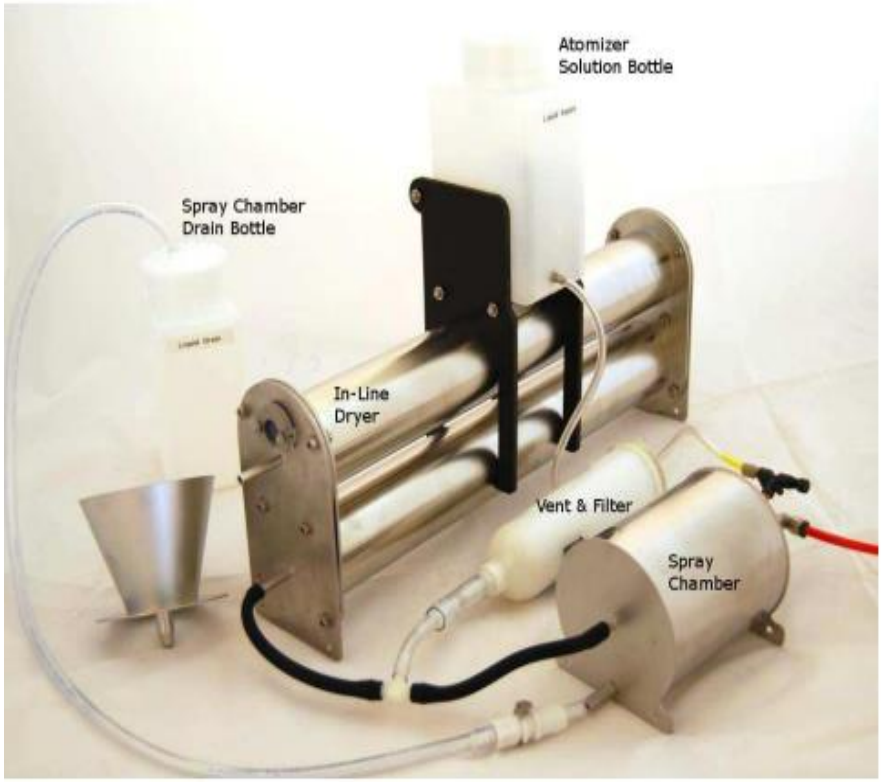

Figure 10. Ammonium sulfate particle generating system (Diagram courtesy of Brechtel Inc)

3.6 Online Instrumentation

The particle size distribution and number concentration in the reactor were monitored with a scanning mobility particle sizer (SMPS) (TSI, Minneapolis, MN, USA). Changes in CCN activity of the particles were monitored 7ith a cloud condensation nuclei counter (CCNc) (CCN-100, Droplet Measurement Technologies (DMT), Boulder, CO, USA). Also, gas phase concentrations of NOx (NO +NO_2) and ozone (O_3) in the reactor were monitored for some experiments with chemiluminescence NOx analyzer (Teledyne Model T200, San Diego, CA, USA) and a photometric ozone analyzer (Teledyne Model 400E) respectively. The operating conditions of the primary instruments used in this study are discussed below.

3.7 Scanning Mobility Particle Sizer (SMPS)

An SMPS consisting of a Differential Mobility Analyzer (DMA, model 3080, TSI, Inc) and Condensation Particle Counter (CPC, TSI 3775) connected in series was used to measure aerosol size distribution within the size range of 8 to 685 nm. The DMA operated on scanning voltage mode classified the particles into different size bins according to their electrical mobility. The particles in each size were transmitted to a CPC where they were counted to obtain the number of particles in each size, thus obtaining the size distribution of the sampled aerosol. To accurately operate a DMA in scanning mode, there is a need to account for the probability of some particles having multiple charges due to their size. Multiple charge and diffusion correction were done using the Aerosol Instrument Manager (AIM version 9.0.0) software (TSI). Particle size distribution and number concentration were measured at 3 min intervals using AIM.

3.7.1 Differential Mobility Analyzer (DMA)

A differential mobility analyzer uses particle's electrical mobility to extract a known size fraction from an incoming polydisperse aerosol. A flow schematic of a typical DMA is shown in Figure 11. The polydisperse aerosol coming into the instrument is first separated by an impactor to remove larger particles by inertial impaction. The aerosol is then introduced into a radioactive krypton (Kr-85) Bipolar Charger (or neutralizer), which establishes charge equilibrium on the particles by exposing them to a high concentration of bipolar ions. The aerosol and the ions from the neutralizer collide by random motion to reach charge equilibrium. On attaining charge equilibrium, the aerosol flows into the top of the cylindrical electrostatic classifier along the outer diameter where they are exposed to an electric field. Those particles with the right mobility size, traverse the electric field towards the center rod and exit through a narrow gap near the bottom

where the CPC counts them. Particles with greater mobility are attracted to the center of the cylindrical rod, while those with lower mobility are filtered out (Hinds, 1999). The mobility diameter of the particles that enter the narrow gap as described by Equation 3.1 (Seol et al., 2002) depends on their size and number of charges**.**

$$D_m = \frac{2neVL\chi C_c}{3\mu q_{sh} ln(\frac{r_1}{r_2})} \qquad 3.1$$

D_m is the particle's mobility diameter, n is the number of charges, represented by e the elementary charge, V voltage applied to the rod, L is the rod's length, C_c is the Cunningham slip correction, μ is the gas viscosity, q_{sh} is the sheath flow rate, and r_1 and r_2 are the inner and outer radii of the cylinder respectively. χ is the particle's dynamic shape factor which corrects for non-sphericity of some particles. For spherical particles $\chi = 1$, and $\chi > 1$ for non-spherical like soot particles. Non-spherical particles experience extra drag that move them towards the DMA rod (DeCarlo et al., 2005). For this study, the DMA was operated on sheath and aerosol flowrate of 8.0 and 0.8 rpm respectively.

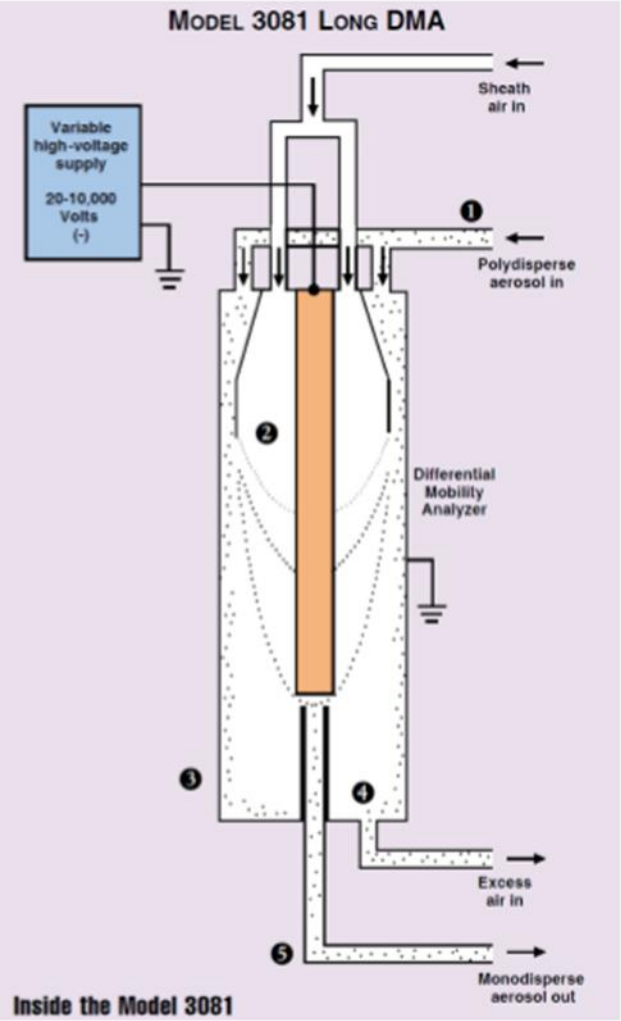

Figure 11. Schematic of the Differential Mobility Analyzer (Diagram courtesy of TSI, Inc.).

3.7.2 Condensation Particle Counter (CPC)

A condensation particle counter (CPC) counts particles by exposing them to a hot saturated vapor stream of butanol or water. The aerosol stream flows through an internal pump of the CPC into a heated saturator, where butanol diffuses into the stream. The aerosol sample and butanol vapor simultaneously flow into a cooled condenser where the butanol vapor becomes supersaturated and condensed on the particles. The particles grow larger and traverse through an optical particle counter (OPC) which counts the particles based on the pulse produced as they

transverse through a laser beam (Hinds, 1999). At a low particle concentration, OPC counts the individual particles based on pulses it produced, but for high particle concentrations, OPC uses total light scattered by the particles to determine its number concentration. CPC (Model 3775 TSI, Inc.) which uses butanol as its working fluid was used for this study. Aerosol sample flows through 3775 CPC at flowrate of 0.3 L/min.

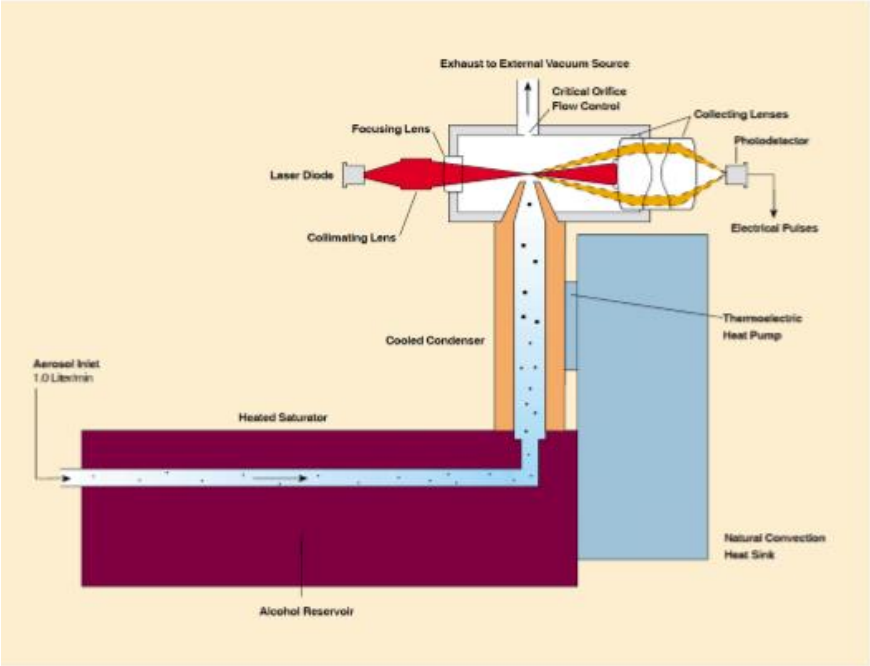

Figure 12. Schematic of the condensation particle counter (CPC, TSI Model 3775) (Diagram courtesy of TSI, Inc.).

3.7.3 Cloud Condensation Nuclei Counter (CCNc)

Cloud condensation nuclei counter (CCN -100 counter, DMT, Colorado, USA) counts the aerosol particles that activated into cloud droplets. The instrument uses the fact that water vapor diffuses faster in the air than heat (Roberts and Nenes, 2005) to create supersaturation (SS) along the centerline of the column (Figure 13). As shown in Figure 11, water vapor diffuses from a warm, wet column along the blue line, while heat diffuses along the red line. Since diffusion of

heat determines equilibrium saturation vapor pressure, it therefore implies that partial pressure at any point along the centerline where the aerosol flows through, for example, point C will be higher than saturation vapor pressure at that point. To achieve equilibrium, water vapor will condense on particles flowing along the centerline of the column and cause the particles to undergo unstable growth into cloud droplets. The particles that grow into cloud droplets are counted by an OPC located at the bottom of the column. The principle used by OPC to count particles has been explained in section 3.7.2.

The SS created along the column depends on total flowrate, operating pressure, and the temperature difference (ΔT) between the top and the bottom of the column. At a fixed flowrate, changing ΔT changes SS. ΔT could be varied continuously to obtain CCN concentrations at different SS, but as explained by Moore and Nenes (2009), a reasonable amount of time is required to stabilize temperatures along the column. Data collected during this period is usually not used. For this reason, the CCN counter was operated at a fixed SS for all the experiments. The instrument was calibrated for a flowrate of 500 vccm (volume cubic centimeter per minute).

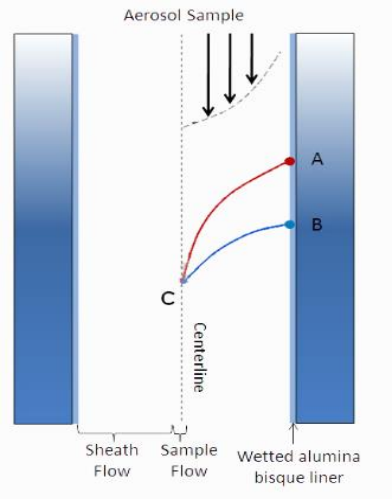

Figure 13. Schematic of supersaturation is generation in the in CCN-100 counter (Diagram courtesy of DMT). The red curve shows the diffusion of heat, while blue curve shows the diffusion of water vapor

3.8 Experimental Procedure

Before each experiment, the chamber was cleaned for several hours (5-7 hours) by heat (40°C), UV radiation and continuous flushing with dry and particle free air to minimize background particles and other contaminants from the previous experiment. After cleaning was done, the concentrations of NO_x and O_3 contained in the air in the chamber were below 0.5ppb. Depending on the experiment being conducted, injection was done in the following order.

1. Clean air
2. Ammonium sulfate particles
3. Diesel exhaust (particles and gases)
4. α-pinene

The purified air was injected into the reactor bag through a 0.5″ outer diameter (OD) stainless steel tubing at a 120SLPM for about an hour. Then, ammonium sulfate particles were injected until the desired mass (18-149µgm^{-3}), and number (32×10^3- 67×10^3 cm^{-3}) concentrations

of $(NH_4)_2SO_4$ particles were in the chamber. The injection of ammonium sulfate took approximately 0.5-2 hours. After injection of ammonium sulfate particle, diesel exhaust from the tailpipe of the engine was injected into the chamber through a 2m heated transfer line for 10-15 minutes until the desired mass (7 – 188μg m^{-3}) and number (54×10^3 -$22\times10^4 cm^{-3}$) were in the chamber. When the desired mass and number concentration of diesel exhaust was in the chamber, 2μl of α-pinene (Aldrich Chemical Co., Milwaukee, WI) was volatilized by passing clean air at a flow-rate of 20SLPM through a heated U-tube (see Figure 7) containing α-pinene and flushing it into the chamber for about 8-12 minute. After injecting all the particles and vapors, an additional air was injected at a flow-rate of 40-60SLPM for about 12minutes. The additional air was injected to allow for proper mixing in the chamber. After the additional air was injected, the UV light was quickly turned on to initiate photochemical aging for the experiments conducted under UV. Experiments were performed at several initial diesel and ammonium sulfate particle concentrations (see tables in chapter 5 for more detail). The experiments lasted for about 4-6 hours and were terminated when the final reactor volume reaches ~ 1/4 of its maximum value.

The size and number of particles in the chamber were measured every 3 minutes by a scanning mobility particle sizer (SMPS). Changes in CCN activity of the particles were monitored every 1 second with a CCN counter (CCN-100, DMT). Gas phase concentration of NOx and ozone (O_3) were monitored every 10 seconds for some experiments with NOx analyzer and O_3 analyzer respectively. For most of the experiments, the temperature in the chamber started at 23^0C and increased to about 32^0C due to UV radiation.

CHAPTER IV

DATA ANALYSIS METHODS AND TYPICAL RESULTS

This study aims to determine the secondary organic aerosol (SOA) formation and the cloud condensation nuclei activity of aged diesel exhaust particles. All experiments were conducted by mixing diesel exhaust particles with air, adding ammonium sulfate particles and/or α-pinene vapor, and exposing the mixture to two atmospheric relevant conditions namely UV radiation and dark conditions. The UV-radiation and dark conditions represent daytime and nighttime respectively. To quantify the SOA formation of aged diesel exhaust, number concentration and the size distribution of the particles in the chamber measured by a scanning mobility particle sizer (SMPS) was converted to total mass concentration by assuming particle density of $1 g/cm^3$. The determined mass was corrected for particle wall loss to account for the mass of the particles deposited on the reactor's wall. The changes in CCN activity of the particles in the chamber was determined by aligning the cloud condensation nuclei (CCN) concentration measured by the CCNc with the raw SMPS data to estimate kappa values, activation ratio and critical diameter of the particles (Moore et al. 2010).

4.1 Number Concentration

Figure 14 shows the number concentration for typical diesel exhaust experiments conducted under UV-radiation (triangle) and dark conditions (cross), respectively. As shown in Figure 14, the number concentration of the particles in the reactor decreased with time for both conditions (UV and dark conditions) due to the coagulation between particles and deposition of the

particles to the reactor's wall. The coagulation rate in the reactor is affected by the particle number concentration and size, while the rate deposition of particles to the reactor's wall is influenced by diffusion, particle size, size of the reactor, and charged wall (Wang et al., 2014). In all the experiments conducted, the number concentration of the particles in the chamber decreased with time.

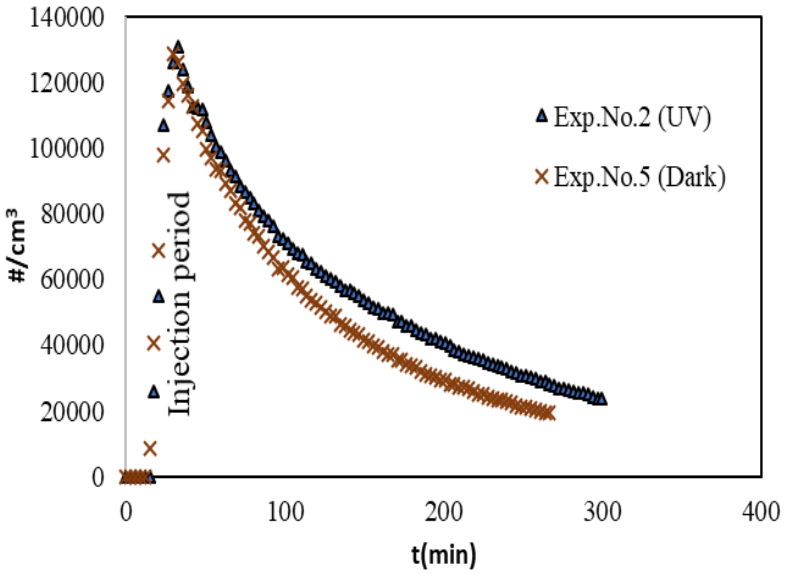

Figure 14. Number concentration of diesel particles under UV condition (triangle) and dark condition (cross).

4.2 Particle Size Distribution

Figures 15 and 16 show typical size distributions of the diesel exhaust particles aged under UV- radiation (Figure 15) and dark conditions (Figure 16). The size distribution of the particles during injection were observed to be unimodal with a peak at approximately 80 nm. The difference in initial number concentration for both experiments was due to difference in injection time. The initial size distribution labelled time "0" in Figure 15 (yellow square) and Figure 16 (blue

triangle) is the time after injection plus 12 minutes required for the diesel exhaust to mix with air in the chamber. The subsequent time are in Figure 15 and 16 are times after time "0".

For the UV experiments, the particles' mean diameter (D_p^{mean}, or peak) shifted towards the larger particle size (Figure 15) due mainly to the condensation of semi volatile compounds on the particle, as well as a small contribution from coagulation of the particles. In the experiment shown in Figure 15, this shift was from 88 nm at t=0 to 111nm after 240min. The peak of the distribution shifts toward larger sized particles because small particle grows relatively more than larger particles do when they absorb the same amount of condensing material (Rose et al., 2006). As the smaller particles grows, the number of smaller particles reduce in contrast to that of larger ones and the mean diameter shift towards larger particle (Rose et al., 2006), Additionally, the shift in the mean diameter could be due scavenging of the smaller particles by the larger particles as they coagulate. Leskinen et al (2007) observed a related shift when particles from diesel engine were exposed to sunlight in an outdoor environmental chamber.

The shift of particles' size distribution toward the larger particles size was more pronounced for all the UV experiments than the dark experiments, which typically saw a change in Dp^{mean} of only 86-90nm. The reason for the obvious shift in size distribution observed for all UV experiments could be attributed to the condensation of the semi-volatile compounds formed by

Photo-oxidation of diesel exhaust on the particles. There was an increase in D_p^{mean} whenever diesel exhaust, whether alone or mixed with ammonium sulfate particles and/or α-pinene vapor, were exposed to UV radiation.

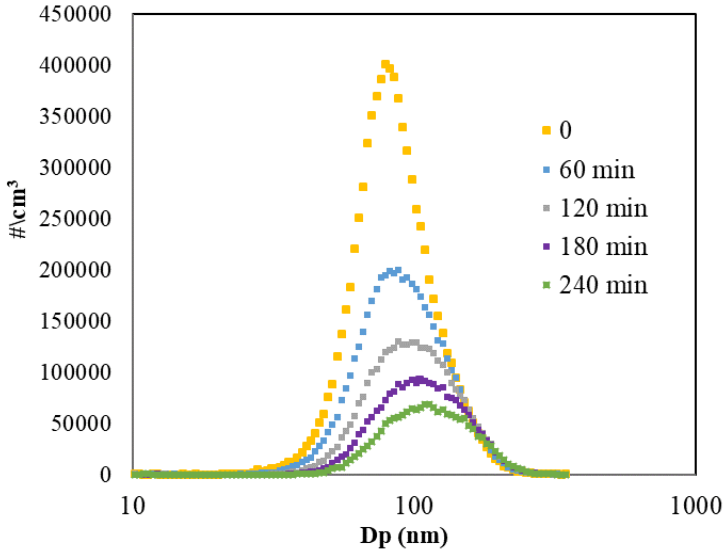

Figure 15. Time-series of particle size distribution in the chamber under UV condition for experiment number 2.

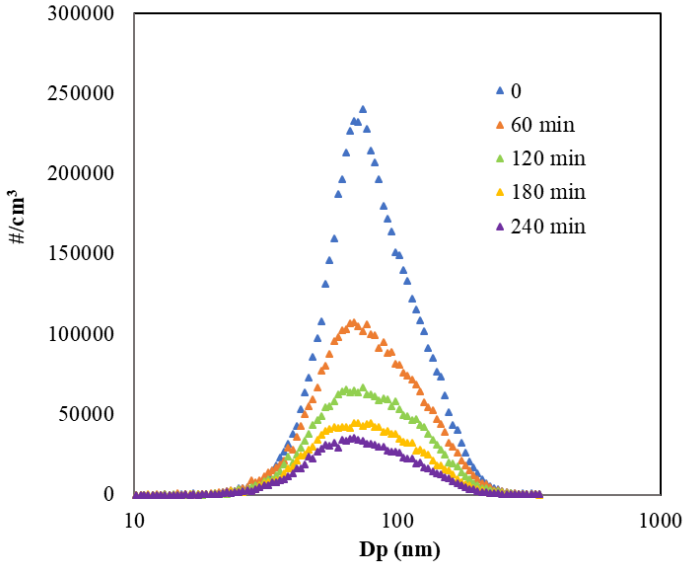

Figure 16. Time-series of particle size distribution in the chamber under dark condition for experiment number 4.

4.3 Quantifying Particle Growth by Mass

To accurately determine total particle mass growth (Secondary Organic Aerosol, SOA formation**),** the mass of the particles lost to the wall due to deposition was accounted for (wall loss correction). Note that the mass lost to the chamber's wall from condensable vapors was assumed to be negligible. The wall loss correction procedures are outlined below.

The loss rate constant (k_w) of particles in the chamber was determined from ammonium sulfate particles experiments performed. The average loss rate constant (k_{wavg}= 7.3×10^{-5} s^{-1}) determined from the ammonium sulfate experiments conducted was taken at the best estimate of the particle loss rate in the chamber. The two other loss rates k_{wlower} (5.7×10^{-5} s^{-1}), k_{wupper}(8.9×10^{-5} s^{-1}) were determined based on the range of the result from the experiments. The particles mass lost to the reactor bag wall at time t, ΔM_t (μgm^{-3}) was calculated from

$$\Delta M_t = k_{wavg} M_t \Delta t \qquad 4.1.$$

where ΔM_t is the mass lost during a given time step, Δt (s), which corresponds to the SMPS measurement interval of 180 seconds, and M_t(μgm^{-3}) is the measured mass at time t.

At the start the of the experiment, (t=0), the corrected particle mass was set equal to the measured mass

$$M_{corrected,t0} = M_{t0} \qquad 4.2$$

where $M_{corrected,\ t0}$ is the initial corrected particle mass and Mt0 is the initial measured particle mass, both at time t0=0. The total particle mass lost to the wall, $M_{lost,\ t}$ was also initialized at time zero

$$M_{lost,t0} = 0 \qquad 4.3$$

Since the total particle mass deposited on the wall is cumulative, the total mass of particle at latter time was obtained by the equation below

$$M_{lost,t} = M_{lost,t-\Delta t} + \Delta M_t \qquad 4.4$$

where $M_{lost,t}$ is cumulative particle mass on the reactor's wall at any time, t. $M_{lost,t-\Delta t}$ is the cumulative mass on the reactor's wall before time t. Recall that measurements are taken every 180seconds. The "corrected mass" was then obtained by adding the total mass lost to the measured mass at a given time

$$M_{corrected,t} = M_{lost,t} + M_t \qquad 4.5$$

To estimate uncertainty in corrected mass values, the $k_{wupper}(8.9\times10^{-5}\ s^{-1})$ and k_{wlower} $(5.7\times10^{-5}\ s^{-1})$ loss rate constants were used in equation 4.1 to determine "upper corrected mass" and the "lower corrected mass" values from equations 4.2-4.5.

A typical time-series of measured particle mass and corrected particle mass for diesel exhaust experiments conducted under UV-radiation and dark condition are shown in Figure 17 and 18 respectively. The curve labeled "measured mass" in Figures 17and 18 represent measured mass without wall loss correction. The curves labeled "corrected mass", "lower corrected," and "upper corrected mass" represent measured mass corrected for particle wall loss rate (see Equations 4.1 to 4.4 for the procedures used).

Although wall loss rate values (k_w) used in this study and the assumption of negligible mass loss due to condensable vapor may represent some level of uncertainty in quantifying diesel particle growth, however, there are two crucial points to be drawn from Figures 17 and 18. First, exposing diesel exhaust to UV radiation resulted to significant increase in corrected mass. As shown in Figure 17 ''corrected mass" (orange square) increased from 81µg/m^3 to about 102

$\mu g/m^3$ for this UV experiment after four hours of aging. This represents 26 % increase in mass after five hours. Weitkamp et al (2007) observed a similar trend in Figure 17 but reported a 60% increase in mass after five hours of aging. The trend (increase in corrected mass with time) shown in Figure 17 was observed for all experiments conducted under UV condition.

Second, the corrected particle mass decreased for all dark experiments. As shown in Figure18 (orange triangle), the corrected particle mass decreased from 80 $\mu g/m^3$ to 60 $\mu g/m^3$ after four hours. Since "corrected mass" should be equal to the initial mass (80$\mu g/m^3$) after wall loss correction for dark experiments, it, therefore, implies that depositional wall losses may have been underestimated. Assuming this to be the case, the corrected mass has been underestimated by 25% in Figure 18 (blue triangles). The trend (decrease in corrected mass with time) was observed for all dark experiments conducted. As a result SOA growth for UV experiments may also have been underestimated due to the wall loss correction used in this study.

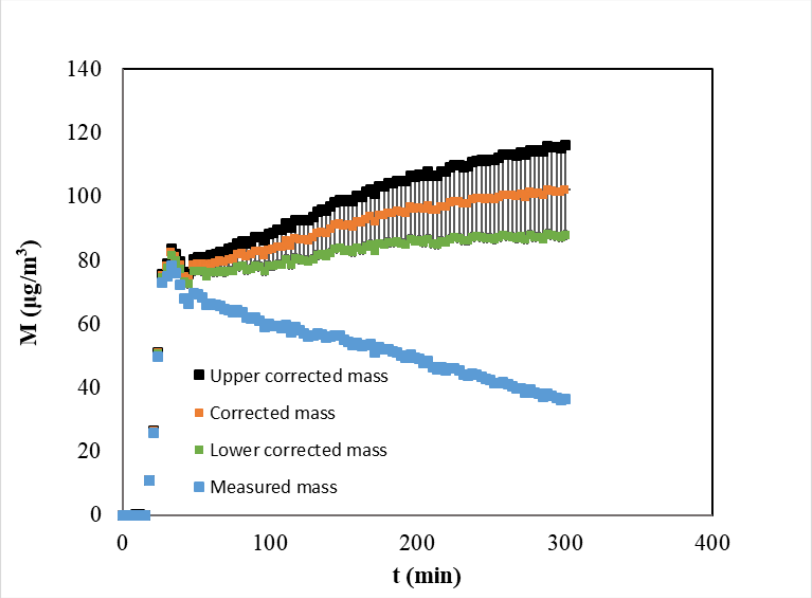

Figure 17. A typical time-series of measured particle mass, (blue square) and particle wall-loss corrected measured masses of UV experiment (Exp.No.2). Lower corrected mass (green square), upper corrected mass (black square) and corrected mass (Orange Square)

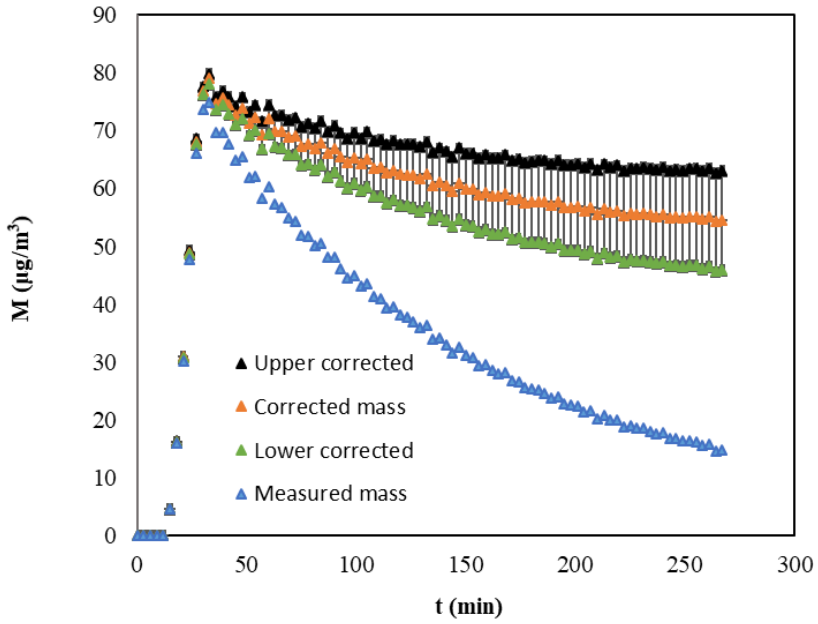

Figure 18. A typical time-series of measured particle mass, (black triangle) and particle wall-loss measured masses of dark experiment (Exp.No.5). Lower corrected mass (green triangle), upper corrected mass (black triangle) and corrected mass (orange triangle)

4.4 Normalized Mass

Results from different experiments were compared by using a normalized mass. This was done to eliminate the influence of conducting the experiments with different initial particle mass will have on particle growth or SOA formation result. Since SOA formation results from the vapor in the diesel exhaust, injecting more particle mass could correspond to more vapor and SOA formation. The normalization procedures for experiments without ammonium sulfate seed particles (diesel exhaust alone and diesel exhaust with alpha-pinene) were the same, but with a slightly different procedure for experiments with ammonium sulfate (diesel exhaust with ammonium sulfate particle and diesel exhaust with ammonium sulfate and alpha-pinene) as described in the following paragraphs. For the experiments, we assumed 12 minutes after injection to be the time required for particles and air injected into the reactor bag to mix (See Figures 19 for the

labels of injection and mixing time) and designate this as time zero, t_0. The assumption was used consistently in all the calculations.

For experiments without ammonium sulfate seed particles, normalization was done as follows. The corrected mass at time zero was taken as the initial mass, M_0

$$M_0 = M_{corrected,t0}$$

Since particles in these experiments are initially composed of only diesel soot, the initial diesel particle mass is the same as the total initial particle mass

$$M_{D0} = M_0$$

Which was then used to normalize the corrected mass values at all times

$$M^*_t = \frac{M_{corrected,t}}{M_{D0}} \qquad 4.6$$

Where M^*_t is the normalized particle mass at time t.

For experiments with ammonium sulfate seed particles, the initial particle mass at time zero, M_0, contains both ammonium sulfate and diesel particle mass

$$M_0 = M_{A0} + M_{D0}$$

where M_{A0} is the initial mass of ammonium sulfate. Therefore, for these experiments, normalization required additional steps to calculate the initial diesel particle mass. Initial diesel mass was calculated by subtracting the ammonium sulfate mass from the total initial mass

$$M_{D0} = M_0 - M_{A0}$$

Similarly, the carbonaceous mass in aged particles can be determined by subtracting ammonium sulfate mass from the total corrected mass

$$M_{D,t} + M_{SOA,t} = M_{corrected,\,t} - M_{A0}$$

The normalized mass can then be calculated as

$$M^*_t = (M_{corrected,\,t} - M_{A0})/M_{D0}$$

Additionally, diesel and ammonium sulfate mass fractions of the initial mass, f_{DO} and f_{A0} respectively, can be calculated from

$$f_{D0} = M_{D0}/M_0$$

$$f_{A0} = M_{A0}/M_0$$

Figure 19 shows a typical normalized graph before truncating the negative reaction time. The negative time on the abscissa (negative x axis) indicate particles injection time plus the time taken for the particles to mix in the chamber. Time zero is taken as start time for the experiment. Subsequent normalized mass figures presented in this paper will start from time zero.

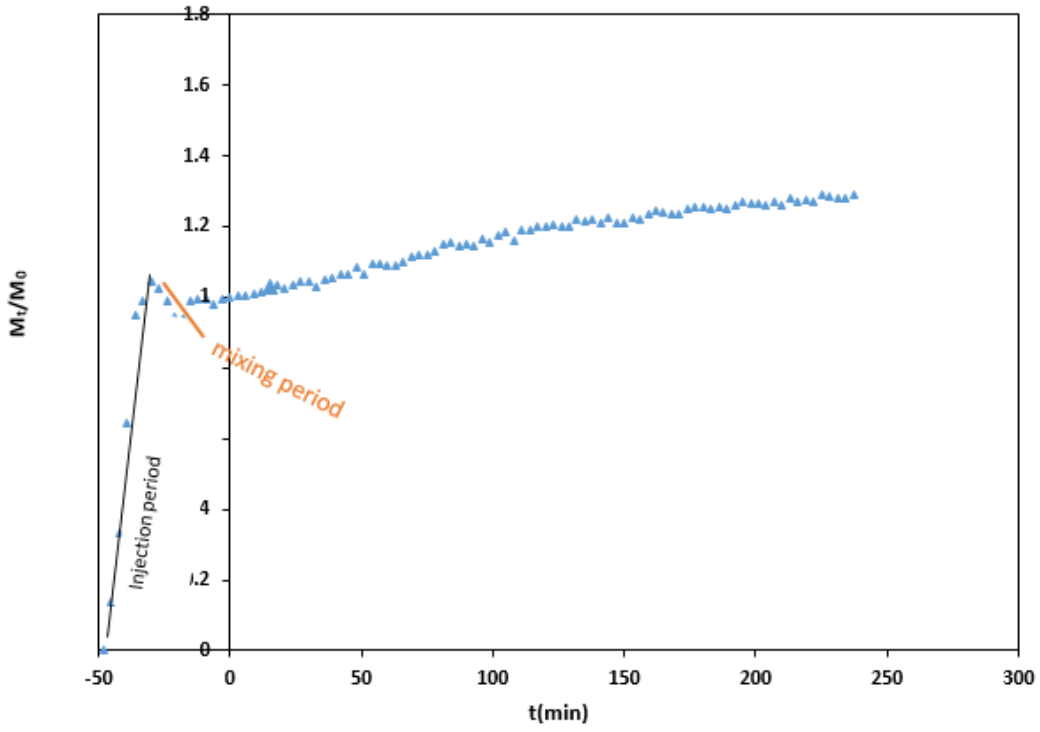

Figure 19. Typical normalized mass showing time and mass during particle injection.

4.5 Quantifying the Cloud Condensational Nuclei Activity

The changes in CCN activity of the aged diesel exhaust particles were characterized by determining CCN based kappa value (κ_{CCN}), critical diameter (Dpc), and activation ratio of the particle with times. Critical diameter is the smallest diameter in the sampled size distribution that can act as CCN. Activation ratio (CCN/CN) is the fraction of the total number concentration acting as CCN. Kappa as explained in section 2.4 quantify the water uptake characteristics and the CCN ability of aerosols. Kappa values can be determined experimentally by fitting CCN data measured by the CCN counter (Petters and Kreidenwies, 2007) Since the SMPS used for this study was operated in scanning mode, the SMPS and CCN data were aligned with Scanning Mobility CCN Analysis (SMCA) method and program developed by Moore et al. (2010). The SMCA program uses the SMPS and CCN counter time to align the data measured by the two instruments (SMPS and CCN counter time was synchronized before the start of all experiments). After aligning the raw SMPS and CCN data, the program also performs multiple charge correction and curve fitting of the data to determine critical diameter and activation ratio. The critical diameter determined from SMCA was used in the equation shown below to calculate κ_{CCN}.

$$\kappa_{CCN} = \frac{4A^3}{27D_{pc}^3 \, ln^2 s_C} \qquad 4.7$$

$$A = \frac{4\sigma_{wo} M_w}{RT\rho_W} \qquad 4.8$$

Where D_{pc} is the critical diameter of the particles, M_w=18.02g/mol is the molar mass of water, σ_{wo}=0.072Jm^{-2} is the surface tension of the water-air interface, ρ_W=1g/cm^3 is the density of water, R is the universal gas constant, T is temperature, S_C critical saturation ratio.

CHAPTER V

EXPERIMENTAL RESULTS

This chapter presents and discusses the results of the experiments conducted for this thesis. The results of four sets of experiments will be presented.

1) diesel exhaust
2) diesel exhaust + α-pinene
3) diesel exhaust + ammonium sulfate seed particle
4) diesel exhaust + α-pinene + ammonium sulfate seed particle

5.1 Diesel Exhaust Experiments

The growth and CCN activity of diesel exhaust particles were investigated by adding diesel exhaust to the chamber containing only clean air (no other particles or gases present). A total of nine diesel exhaust experiments were conducted. Seven runs were performed under UV condition and two under dark condition. The experiments were conducted with the initial mass and number concentrations' ranging from 34 – 185 μg m^{-3} and 1×10^4 - 17×10^4 cm^{-3} respectively. CCN activity of the aged diesel exhaust particles was investigated at different CCN counter supersaturation (0.16 -0.88%) setting. The typical temperature observed in the chamber during the experiments were in the range of 23-32 ^{0}C. For one run, (Experiment number 16, see Table 2) the temperature in the chamber was decreased from 28 ^{0}C to 20 ^{0}C after 2 hours of the reaction. Also, the SS of CCN counter for Exp16 changed from 0.88% to 0.6% after about 9 minutes into the reaction.

5.1.1 Normalized Particle Mass in Diesel Exhaust Experiments

Table 2 shows the list and summary of the experimental conditions of all the diesel exhaust experiments performed. The percent change in mass shown in Table 2 was calculated with the equation shown below.

$$\Delta M\% = \frac{(M_{end} - M_0)}{M_0} \times 100\% \qquad 5.1$$

Where M_{end} is the final corrected mass at the end of the experiment (note that different reaction time is being used for Mend, time of ranging from 4-6 hours) and M_0 is the initial corrected mass at the start of the experiment (For the procedure on how M_0 was determined, see section 4.4.). As shown in Table 2, the photo-oxidation of diesel exhaust with UV-radiation increased the particle mass between -2 to 39 %. For the experiments performed under dark condition (Exp .4 and 5), particle mass decreased by 27 to 34 %.

Table 2. Summary of Diesel Exhaust Particle Experiments and the Experimental Conditions.

Experiment Number	UV/Dark	Initial M ($\mu g/m^3$)	Initial N ($\#/cm^3$)	ΔM (%)	SMPS Particle Size Range (μm)	Temperature (^0C)	CCN Counter Supersaturation SS (%)
1	UV	29	4.6×10^4	-2	8-352	23-32	0.16
2	UV	74	11×10^4	37	8-352	23-32	0.6
3	UV	34	5.4×10^4	12	8-352	23-32	0.74
4	Dark	62	9.0×10^4	-34	8-352	23-32	0.74
5	Dark	74	9.3×10^4	-27	8-352	23-32	0.88
6	UV	78	12×10^4	39	8-352	23-32	0.88
16	UV	120	23×10^4	6	8-352	Reduced from 28 °C to 20°C after 2 hours	0.88 and 0.6
17	UV	188	15×10^4	9	8-352	25-28	No CCN
18	UV	78	14×10^4	23	8-352	25-30	No CCN

Figure 20 shows the normalized mass of the diesel exhaust experiments conducted. Dark experiments (unfilled triangles) consistently showed a decrease in mass by a factor of about 0.3. By exposing the diesel exhaust (gases+ particles) to a UV radiation, the total mass of particles increased by a factor of 1.0-1.4. The photochemical reactions initiated by the UV formed products that condensed on the particles to increase the total mass of the particles. Lee et al., (2004), reported a 100% increase in mass of diesel exhaust particles after 5 hours of exposing them (diesel exhaust particles) to natural sunlight. The difference between the percent change in mass observed in the experiments presented in this thesis and that reported by Lee et al., (2004) could be attributed to the following:

1. The difference in emission rate of the two-different diesel engine used. Lee et al., (2004) used a 1980 Mercedes Benz 3000 SD, while a 2005 Kubota four-cylinder was used for this study
2. The difference in diesel fuel sulfur (for this study, the sulfur content was 0.0015w% and 0.05w% for Lee et al., (2004)),
3. Different exposure method (While this study exposed the diesel exhaust to UV light, Lee et al., (2004) used natural sunlight).

While the magnitude of particle growth was different, the general trend of an increase in mass was observed by both studies (Lee et. el, 2004 and this thesis) for UV exposure.

For experiment 16 (purple triangle), the chamber's temperature was reduced from about 28^0C to 20^0C after 2 hours of reaction to investigate the partitioning of diesel exhaust photo-oxidation products between the particle phase and the gas phase. As shown in Figure 20 (purple tri-

angle), the mass of the diesel exhaust particles suddenly increased when the chamber's temperature was reduced indicating condensation of semi-volatile compounds in the gas phase on the diesel particles.

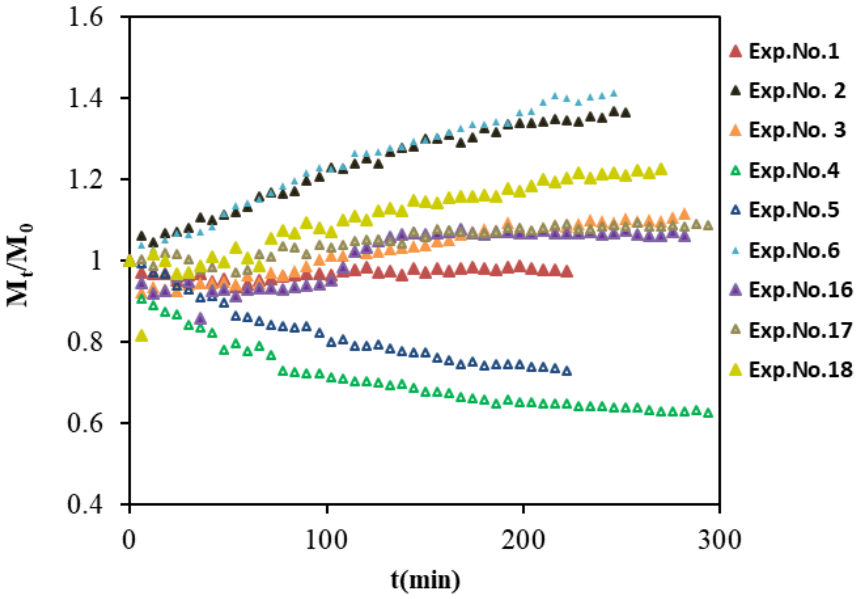

Figure 20. Normalized particle mass in diesel exhaust experiments. Unfilled triangles represent dark experiments, while filled triangles are for UV experiments

5.1.2 Kappa Values in Diesel Exhaust Experiments

Kappa values of fresh and photochemically aged diesel exhaust particles are shown in Figure 21 as a function of reaction time. Diesel exhaust particles were utterly CCN inactive under dark condition (Exp. No.4 orange triangle and Exp No.5, black triangle) as κ_{CCN} were ~ 0 for both experiments. This result confirms that fresh soot is hydrophobic and unable to activate into cloud droplets. This result is consistent with results of many studies, e.g., Zuberi et al. (2005) who showed that hexane soot particles were CCN inactive at about 15% SS.

Aging of diesel exhaust particles in the presence of UV-radiation (Figure 21, filled squares) significantly enhanced CCN activation due to condensation of SOA products formed by UV initiated photochemical reaction. κ_{CCN} was observed to depend on reaction time (UV exposure time). For all UV experiments, κ_{CCN} increased consistently with time because more water-soluble products formed by photooxidation of diesel exhaust condenses on the surfaces of diesel particles. Kappa value only quantifies water uptake ability (solubility) of the particle and doesn't depend on SS setting of the CCN counter.

Kappa value (after 200 minutes reaction time, see Figure 21) was noticeably higher for Exp.No 16(tan square) than other experiments conducted. The explanation for the high kappa value could be due to the increased condensation of soluble products on the particles' surface when the chamber's temperature was reduced deliberately from 28°Cto 20°C after two hours of UV exposure. The decrease in temperature may have allowed slightly more volatile, but more hydrophilic products to condense on the diesel particles, thus increasing their ability to interact with water vapor and activate into cloud droplets. After 200 minutes of aging, the kappa value for the other UV experiments were in the range of 0.02-0.08 (Figure 21). As discussed in section 2.5, kappa values range from 0.5 to 1.4 for highly soluble inorganic salt particles, 0.01-0.5 for slightly hygroscopic organic, and zero for insoluble particle. Our result ($\kappa_{CCN,}$ 0.03-0.08) signifies that aging of the diesel exhaust particles with UV radiation transformed non-hygroscopic (insoluble) diesel particle to slightly hygroscopic particles.

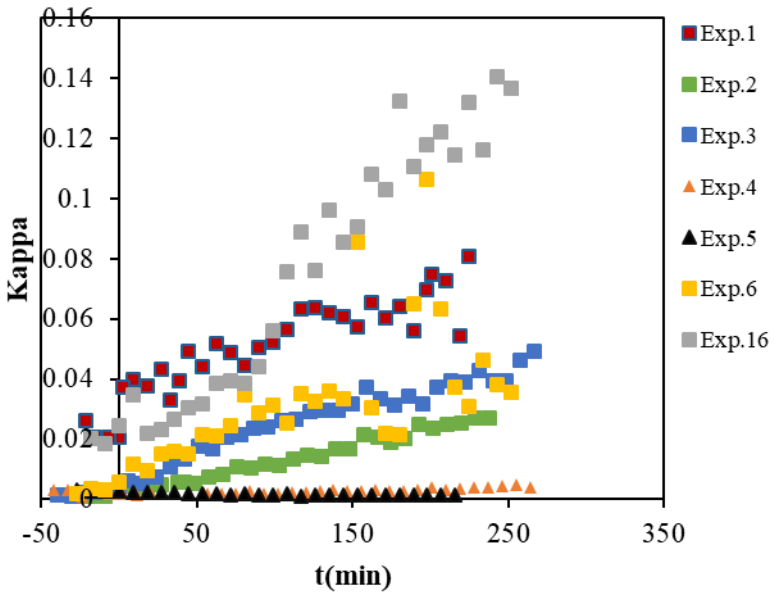

Figure 21. Kappa value for diesel exhaust experiments. Dark experiments (filled triangles) UV experiments (squares)

5.1.3 CCN Critical Diameter in Diesel Exhaust Experiments

The effect of photochemical oxidation on CCN critical diameter (D_{pc}) of diesel exhaust particles is shown in Figure 22. For the two dark experiments conducted, critical diameter seemed to increase with reaction for Exp.5 (light blue triangle) but decreased with time for Exp.4 (orange triangle). The reason for these conflicting results remains unclear.

From Figure 22, it is evident that critical diameter at a fixed supersaturation decreased with reaction time for all UV experiments (filled squares). The D_{pc} were relatively higher at the onset of the experiments, because the particles were unaged diesel soot that is insoluble, which allows only larger particles to act as cloud droplets. As the reaction proceeds, the water-soluble gas phase products formed due to UV radiation condenses on the particles and enable the smaller particle to activate into the cloud droplet, thus reducing the critical diameter. The decline in D_{pc}

of continues throughout the aging process as more water-soluble mass condenses on the diesel exhaust particles.

As expected, the critical diameter for UV experiments was found to depend on the super-saturation setting of the CCN counter because at higher SS, more water vapor is available for activation, then, smaller particles activate. For example, the critical diameter for the experiments conducted at 0.8% SS (Exp.6 and 16) were found to show smaller activation diameter than experiments 1 and 2 (blue squares, green square respectively) conducted at SS of 0.1% and 0.6 % respectively. After 250 minutes aging, particle diameter with the range of 70-80nm (Figure 22, yellow, tan and purple squares) could activate into cloud droplet.

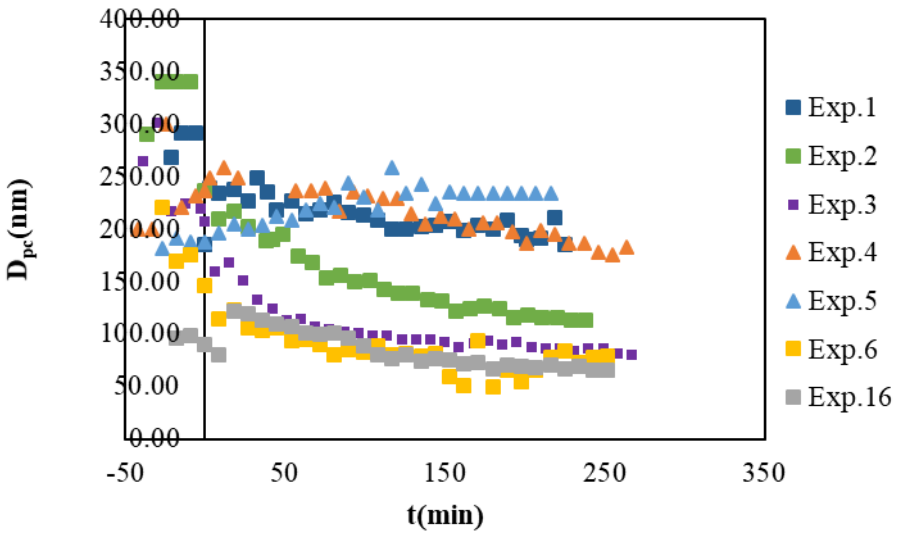

Figure 22. Critical diameter for diesel exhaust experiments. Dark experiments (triangles) UV experiments (squares)

5.1.4 Activation Ratio in Diesel Exhaust Experiments

The fraction of particles that activate (activation ratio) depends on the supersaturation and on the particles' size and chemical composition. At the beginning of all the experiments, only a

small fraction (0- 10 %) of the entire diesel exhaust particles activated into cloud droplets (See Figure 23). Over time, as the diesel exhaust particles grow(size) due to coagulation and condensation and their composition changes due to chemical aging, the fraction that activates will increase. For the two darks experiments conducted, one experiment (Exp.5, blue triangle) showed < 1% activation after 200 minutes. The other dark experiments (Exp. 4, orange triangle) increased to about 10% activation. The reason for the discrepancies in the activation ratio for the two dark experiments remain unclear.

The observation of an increased activation with UV exposure (reaction time) was consistent with all UV experiments. As proposed by Weingartner et al. (1997), the increase in activation ratio with UV exposure could be attributed to the condensation of photochemically produced compounds on the particle surface and the photolysis of polycyclic aromatic hydrocarbon (PAH), found in diesel particles. The contributions of condensation of soluble compounds and photolysis of the PAH changes the chemical composition of the diesel exhaust particles to something more hydrophilic and enable them to retain water vapor and activate into cloud droplets. Also, the growth in particle size observed for all UV experiments could also be a factor contributing to the increase in activation ratio with reaction time observed for all UV experiments

The activation ratio was found to increase with SS setting of the CCN counter. For example, as the supersaturation ratios used for UV experiments 1, 2, 3, and 6 increased (0.16%, 0.60%, 0.74%, and 0.88%) the activation ratio after 200 minutes of UV exposure also increased (0.1, 0.6, 0.7, 0.75). Also, the effect temperature on CCN activation seems to be evident when the chamber's temperature was reduced from 28 ^{O}C to 20 ^{O}C after two hours of reaction for Exp.16 (tan square). As shown in Figure 23, at the time of the temperature change, the activation

ratio increased more rapidly, reaching 80% of the total diesel exhaust particle activated for Exp.16 after 200 minutes of reactions. The reason for high activation noticeable for Exp.16 could be attributed to more condensation of water-soluble gas product on the particles when the temperature in the chamber was reduced, thus changing both the composition and size of the particles.

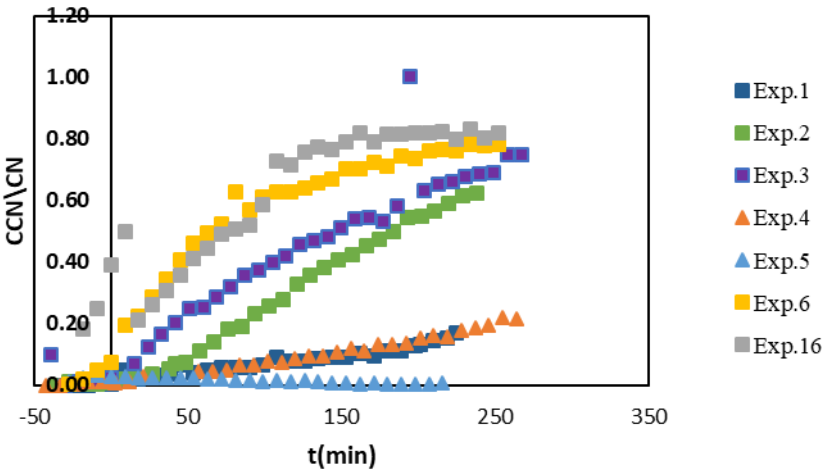

Figure 23. Activation ratio for diesel exhaust experiments. Dark experiments (triangles) UV experiments (squares)

5.2 Diesel Exhaust + α-pinene Experiments

All the experiments (diesel exhaust + α-pinene) were conducted by mixing diesel exhaust with air and flushing a volatilized 2µl α-pinene into the chamber. The concentration of α-pinene injected into the chamber was calculated to be 39 ppbv (see equation 5.2 for α-pinene concentration calculation)

$$ppbv = \frac{volume\ of\ \alpha\text{-pinene vapor}}{\text{volume of air in the reactor bag}} \times 10^9 \qquad 5.2$$

Table 3. Summary of Diesel Exhaust Particle + α- pinene Experiments and the Experimental Conditions.

Experiment Number	UV /Dark	Initial M ($\mu g/m^3$)	Initial N($\#/cm^3$)	ΔM%	SMPS Particle Size Range (μm)	α-Pinene Conc. (ppbv)	Temperature (^0C)	CCN Counter Supersaturation SS (%)
12	UV	97	16×10^4	70	8-352	39	23-32	0.88
13	UV	107	15×10^4	45	8-352	39	23-32	0.88
14	UV	79	14×10^4	52	8-352	39	23-32	0.88
15	UV	68	7.6×10^4	71	8-352	39	23-32	No CCN

The volume of air was taken as the volume of the bag (8 m^3). A total of four experiments with diesel exhaust and α-pinene were conducted. The experiments were conducted with initial particle mass and number concentration ranging between 68 -107 $\mu g m^{-3}$ and 7.6×10^4 - 16×10^4 cm^{-3} respectively. The CCN activity of the diesel exhaust particles aged in the presence of α-pinene and UV radiation was investigated at one SS (0.8%).

5.2.1 Normalized Particle Mass in the Diesel Exhaust + α-pinene Experiments

Table 3 shows the summary of the experimental conditions and percent change in mass of the diesel exhaust aged with α-pinene. As shown in Table 3, the percent change in mass (ΔM %) were in the range of 45-71% when compare to the initial mass of diesel particles. The additional increase in mass observed for the diesel exhaust + α-pinene (see Table 3) when compare to the diesel exhaust experiments (Table 2) could be attributed to the following: extra particle mass from condensing semi-volatile products formed from the photooxidation reactions of α-pinene, additional partitioning to the particle phase of semi-volatile products from diesel exhaust photooxidation, and the SOA formation from the cross photochemical reactions between diesel exhaust components and α -pinene (Lee et al., 2004). In a similar study of diesel exhaust and α -pinene photooxidation Lee et al., (2004) observed up to 400% increase in particle mass, but their study used much larger amounts of a-pinene, about 140ppbv, with diesel particle concentrations, (50-85 $\mu g\ m^{-3}$) comparable to the experiments listed in Table 3. The total SOA yield (Y, α-pinene SOA + diesel exhaust SOA) defined as the ratio of total SOA mass formed (ΔM, or (M_{end}-M_o), $\mu g\ m^{-3}$) to the mass concentration α-pinene consumed (ΔHC, $\mu g\ m^{-3}$), were calculated for this study and compare to that of Lee et al., (2004).

$$Y = \frac{\Delta M}{\Delta HC} \qquad 5.3$$

By assuming that all the α-pinene reacted, the mass of reacted α-pinene was calculated using the equation from Seinfeld and Pandis (1998).

$$\text{Conctration in } \mu gm^{-3} = \frac{PM_{\alpha-pinene}}{8.314\ T} \times \text{mixing ratio in ppm} \qquad 5.4$$

Where P is the pressure (1 atm), T, temperature (K), $M_{\alpha\text{-pinene}}$ is the molecular weight of α-pinene and mixing ratio is the concentration of the reacted α-pinene (ppm). The SOA yield for this study was estimated to be in the range of 0.2- 0.32, while that of Lee et. al., 2004 was 0.2. This thesis and Lee et al., (2004) observed similar total SOA yield.

Figure 24 shows the normalized particle mass in the diesel exhaust + α-pinene experiments. As can be seen, the particle mass increased by 1.4 to 1.7 compared the initial mass of the diesel exhaust particle injected into the chamber. Comparing the normalized mass in Figure 24(Exp.15, mass increased by a factor 1.7) to normalized mass in the diesel exhaust experiment (Figure 20, Exp 4, mass increased by a factor 1.4), we observed that the addition of 39ppbv of α-pinene increases particle mass by 21% after 250 minutes of reaction.

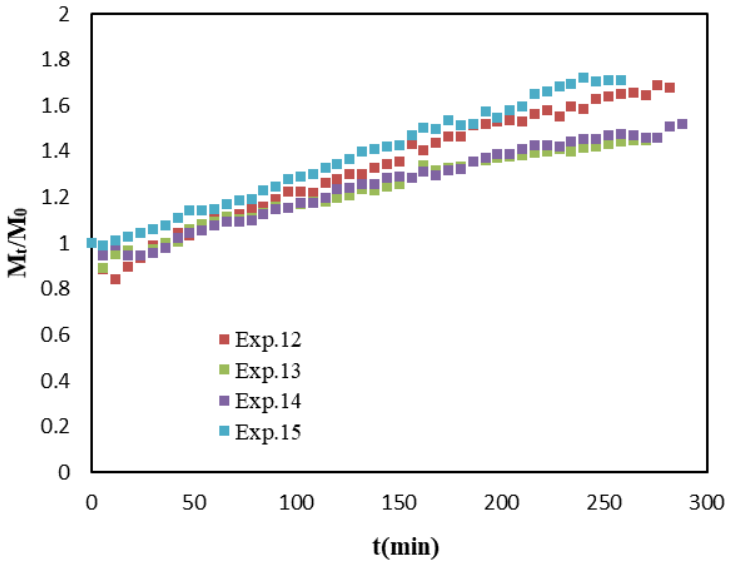

Figure 24. Normalized particle mass in diesel exhaust + α-pinene experiments.

5.2.2 Kappa Values in Diesel Exhaust + α-pinene Experiments

Figure 25 shows kappa value for diesel exhaust particle aged in the presence of UV radiation and α-pinene (39ppbv). All the experiments were conducted at the same temperature range (see Table 3). The kappa values were initially~ 0 at the start of the experiments because diesel particles are hydrophobic and unable to activate. As the UV initiated photochemical reaction proceeds, more water-soluble semi-volatile compounds condense on the particles to increase their κ_{CCN}. Kappa value was observed to increase with time reaction (see Fig.25). Comparing the κ_{CCN} of diesel exhaust experiment (Figure 21, κ_{CCN} ranging from 0.03-0.08) to that of diesel+ α-pinene experiment (Figure, 25 κ_{CCN} ranging from 0.08-0.15) after 250 minutes of reactions, we observed about 88% increase in kappa value due the contributions of the SOA formed from the 39 ppbv of alpha-pinene and the diesel exhaust vapor.

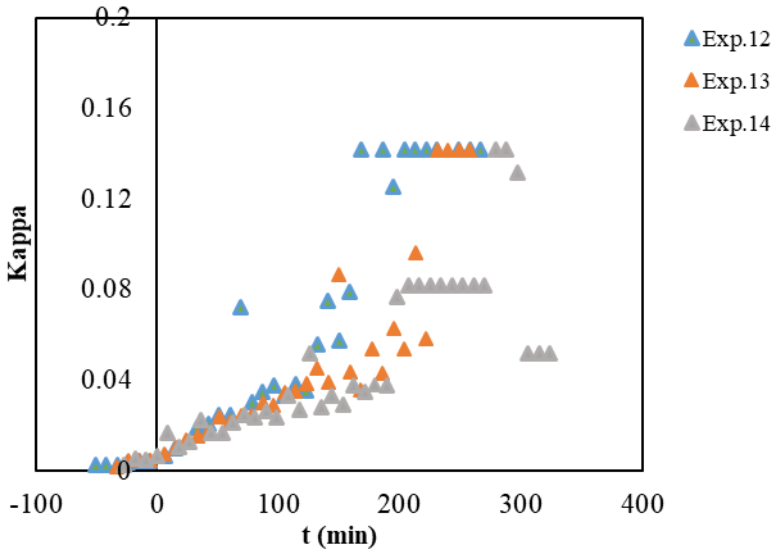

Figure 25. Kappa value for diesel exhaust + α-pinene experiments

5.2.3 CCN Critical Diameter in Diesel Exhaust + α-pinene Experiments

The ability of a particle to act as CCN depends on the particle size (Kelvin effect), solubility (Raoult effects), and the prevailing atmospheric SS. At the start of the experiment, only particles of about 150nm (Figure 26, diamond) could activate because the particles are unaged and only particles of large diameter activate. As the reaction proceeds, the critical diameter decreases because the CCN ability of hydrophobic diesel particles increases with increasing amount of more hydrophilic organic coating material, i.e., increases in SOA mass fraction (Tritscher et al. 2011). The water-soluble gas phase products condense on the particle surface, thus increasing their solubility and CCN ability. After about 5 hours of aging, particle as low as 50nm in diameter could activate into cloud droplet. Comparing the critical diameter for UV experiments in Figure 22 (D_{pc} ranging from 70-90nm) to that in Figure 26 (D_{pc} ranging from 50-60nm), we observed that the addition of 39 ppbv of alpha-pinene decreased the diameter required for activation after 250 minutes of reaction.

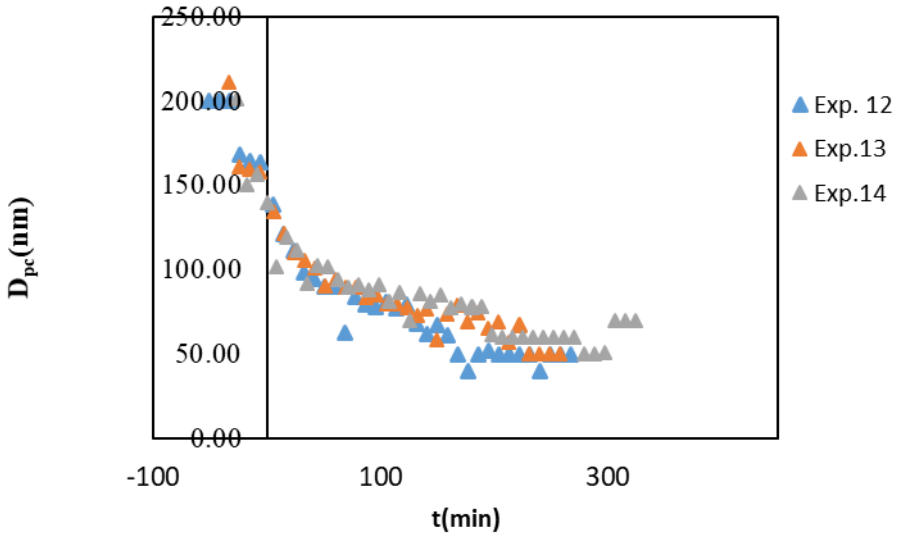

Figure 26. Critical diameter for diesel exhaust + α-pinene experiments.

5.2.4 Activation Ratio in Diesel Exhaust + α-pinene Experiments

The activated ratio of diesel exhaust particle aged in the presence of UV and α-pinene are shown in Figure 27. Activated ratios were ~ 0 at the start of the experiment. The enhancement of hygroscopicity and CCN activation of the particles were observed when the diesel exhaust aerosol and α-pinene vapor are subjected to UV radiation. The activated ratio increased with reaction time. By the end of the experiments (5 hours), ~ 90% of the total diesel exhaust particle formed cloud droplets. The activation ratio for diesel exhaust + α-pinene experiments (Figure 27, 0.78-0.8) after 250 minutes of aging are like the highest ratios observed for diesel exhaust experiment (0.8).

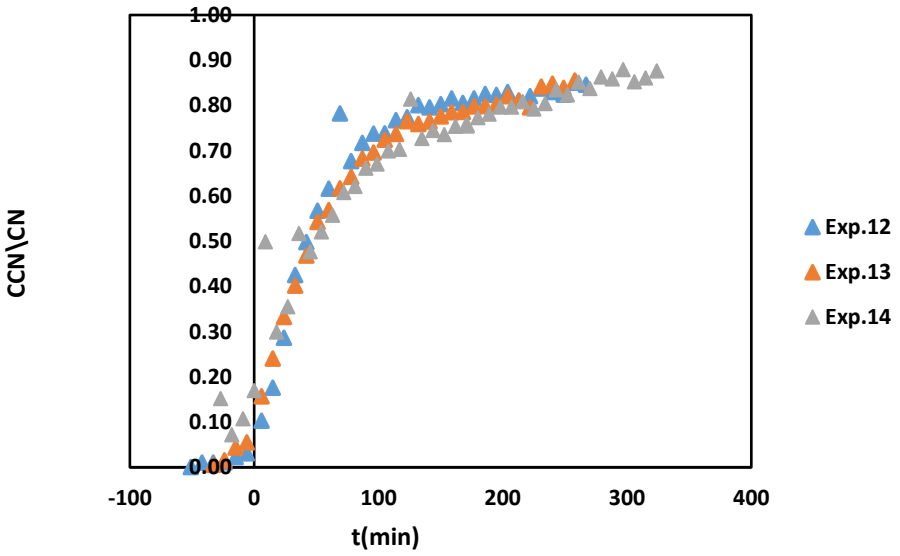

Figure 27. Activation ratio for diesel exhaust + α-pinene experiments.

5.3 Diesel Exhaust + Ammonium Sulfate Seed Particle Experiments

Table 4 shows the list of the experiments conducted using a combination of diesel exhaust and ammonium sulfate seed particles and their experimental conditions. A total of 10 experiments were performed. Eight of the runs were performed under UV condition and two runs

under dark condition. These experiments were conducted to investigate how coagulation between diesel and ammonium sulfate particle impact both CCN activity of hydrophobic diesel particle, as well as diesel particle mass growth, at different ammonium sulfate mass concentration. Various amount of ammonium sulfate particles and diesel exhaust was injected into the chamber to achieve a range in the ratio between initial ammonium sulfate and diesel particle mass. See Table 4 for the fraction of initial particle mass that was ammonium sulfate particles (initial particle mass contains ammonium sulfate and diesel exhaust particles). The CCN activity of the mixture of diesel exhaust and ammonium sulfate seed particle was investigated at SS of 0.59-0.88% (see Table 4). The temperature in chamber was observed to range from 23 to 32^0C (see Table 4).

Table 4. Summary of Diesel Exhaust with Ammonium Sulfate Particle Experiments and the Experimental Conditions.

Experiment No.	UV/Dark	Initial M(μg/m^3)	Initial N(#/cm^3)	ΔM%	SMPS Particle Size Range (μm)	$(NH_4)_2SO_4$ Mass Fraction	Temperature (^{0}C)	CCN Counter Supersaturation SS (%)
7	UV	25	3.7×10^4	11	8.-352	0.73	23-32	No CCN
8	UV	216	174×10^4	27	8-352	0.69	23-32	0.88
9	UV	129	13×10^4	34	8-352	0.49	23-32	0.88
10	Dark	211	13×10^4	-28	8-352	0.68	23-32	0.88
11	Dark	182	18×10^4	-23	8-352	0.61	23-32	0.88
19	UV	162	15×10^4	72	14-685	0.83	25-30	0.88
20	UV	105	9.6×10^4	93	14-685	0.75	25-30	0.88
21	UV	215	19×10^4	87	14-685	0.36	25-30	0.88
22	UV	174	24×10^4	22	14-685	0.28	25-30	0.639
23	UV	161	27×10^4	33	14-685	0.35	25-30	0.586

5.3.1 Normalized Particle Mass in Diesel Exhaust +Ammonium Sulfate Seed Particle Experiments

The normalized mass of the UV experiments, as seen in Figure 28, universally showed an increase in mass with the range of 11-93 %(See Table 4). Furthermore, changing the mass fraction of ammonium sulfate in initial particle mass does not seem to have an effect on ΔM% (See Table 4). Most of the UV experiments showed mass increase with the range of 11-34% (Experiments, 1, 2,3,22 and 23). In contrast, Experiments 19, 20 and 21. (Dark blue, brown, and green filled square respectively) showed an unusually large increase in mass (72%, 93% and 87% for Exp. 19, Exp.20, and Exp.21, respectively). The reasons for the higher increase in mass observed for these three experiments is still unclear. An increase in sampled size range did not seem to affect condensational growth of the diesel exhaust particle (see Table 4). The effect of temperature on condensational growth was observed not to be significant for UV experiments since there was no significant difference in ΔM% between the experiments conducted under the temperature range of 23-32 ^{0}C (Exp No.7, 8 and 9) to those performed under the temperature range of 25-30 ^{0}C.

When compared to their initial mass, the normalized mass of UV experiment showed an increase in mass by a factor of 1.1-1.9, and the mass of dark experiments was observed to decrease by the factor of 0.9-0.8 (see Figure 28). Comparing the particle mass increase (1.1-1.2) in Figure 28(Exp 8, 9, 23 and 24) to that in Figure 20(1-1.4) after 250 minutes of reaction, it is evident that particle growth was higher for diesel exhaust experiments than when diesel exhaust was mixed with ammonium sulfate seed particles (Figure 28, Exp 8,9,22 and 23).

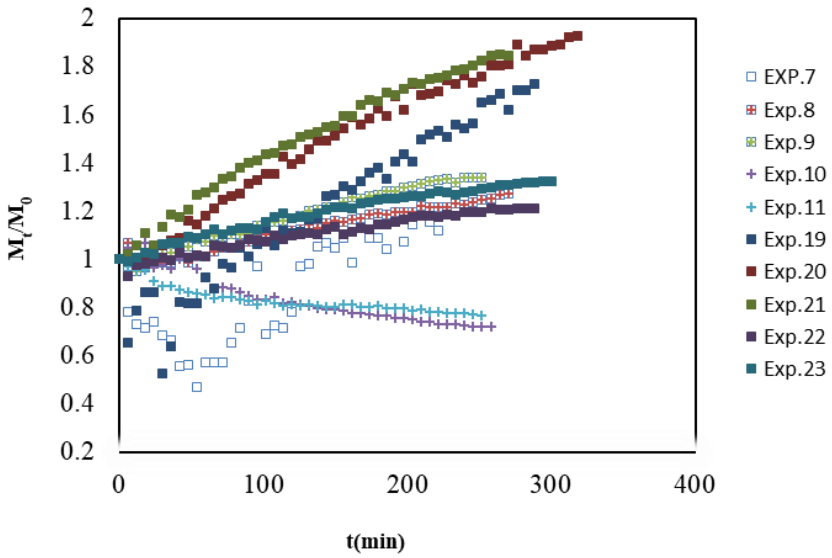

Figure 28. Normalized mass of diesel exhaust and ammonium sulfate particles experiments. Squares for UV and cross for dark experiments.

5.3.2 Kappa Value in Diesel Exhaust + Ammonium Sulfate Seed Particle Experiments

Kappa values for diesel exhaust particles aged with ammonium under dark and UV radiation are compared in Figure 29. Kappa values prior to time zero when only ammonium sulfate particles had been injected were observed to be high due to the solubility of ammonium sulfate particles. For all the experiments in Figure 29, kappa value (not shown because Y axis was truncated) for ammonium sulfate particle were ~0.6. This value is consistent to that reported by Petter and Kreidenwies (2007). After diesel exhaust injection, κ_{CCN} decreased to~ 0. This does not mean that the ammonium sulfate particles stopped activating, but is a result of a single kappa value being calculated for a mixture of two distinct particle populations. For dark experiments (Exp No. 10 and 11), κ_{CCN} remained ~ 0 during the experiments. Unlike the dark experiments,

κ_{CCN} increased from zero when the mixture of ammonium sulfate and diesel exhaust were exposed to UV radiation (Fig.29, diamonds). κ_{CCN} was found to range from 0.02-0.3 for UV experiments (see Figure 30). The variability in kappa values observed for UV experiments seem to be correlated with the ammonium sulfate fraction and the % increase in particle mass. For example, the highest κ_{CCN} values were observed for Exp.No. 19(κ_{CCN} ~ 0.3 after 250 hours) and Exp.No.20 (κ_{CCN} ~ 0.258 after 250 hours), which had high ammonium sulfate mass fraction in the initial aerosol mass (0.83and 0.75) and large increases in particle mass (72% and 93%).

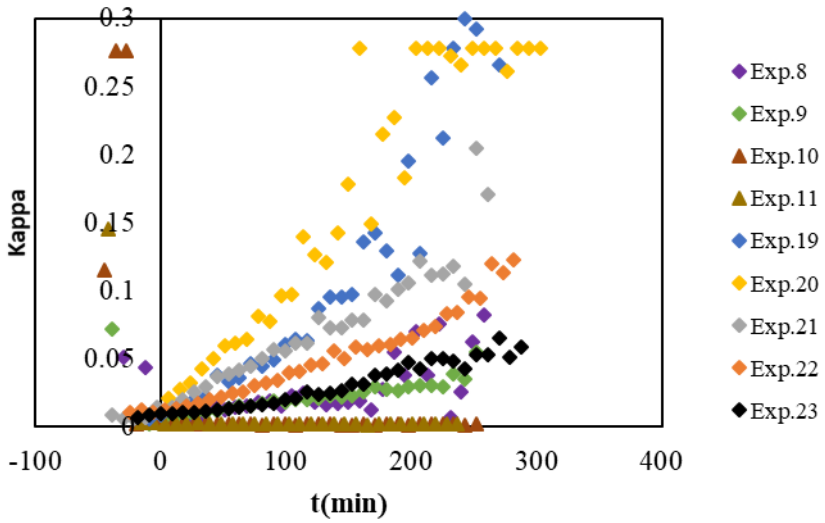

Figure 29. Kappa value in diesel exhaust+ ammonium sulfate seed particle experiments under UV radiation (diamonds) and dark (triangle) conditions.

5.3.3 CCN Critical Diameter in Diesel Exhaust + Ammonium Sulfate Seed Particle Experiments.

The critical diameters of the diesel exhaust + ammonium sulfate seed particle experiments are shown in Figure 30. Prior to time zero, the critical diameter was initially low (about 45nm, Figure 30) for all the experiment due to the ammonium sulfate particle. The injection of diesel exhaust particles increased the critical diameter within the range of 130nm -190nm. For

the dark experiments (triangle), the critical diameter remains approximately constant with time. In contrast, the critical diameters decreased with reaction time for all UV experiments due to condensation of the water-soluble semi-volatile compound on the diesel particles. After 250 minutes of aging, the critical diameter was with the range of 50- 100nm. The D_{pc} of the experiments containing higher initial ammonium sulfate mass fraction and higher mass growth (Exp 19 and 20) showed the largest decrease in D_{pc} (50nm after 250 minutes) when compared to other experiments.

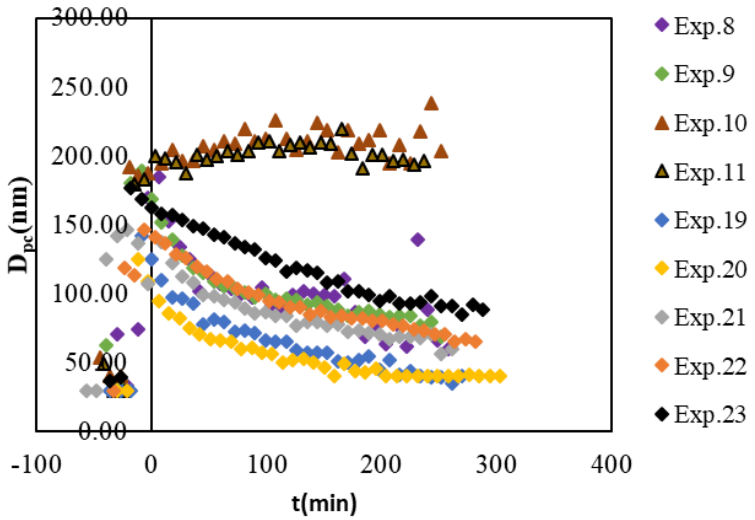

Figure 30. Critical diameter in diesel exhaust+ ammonium sulfate seed particle experiments under UV radiation (diamonds) and dark (triangle) conditions.

5.3.4 Activation Ratio in Diesel Exhaust + Ammonium Sulfate Seed Particle Experiments

Figure 31 shows the time series activation ratio of the diesel exhaust + ammonium sulfate seed particle experiments. At the start of the experiment, the activation ratio was within 0.8-0.9 due to activation of ammonium sulfate particle. When diesel exhaust particles were introduced into the chamber, the activation ratio dropped to about 0.08 -0.28 (see Figure 31) due non-activation of hydrophobic diesel exhaust particles. As the mixture of diesel exhaust and ammonium

particle were continuously aged with a UV radiation, the semi-volatile compound formed in the gas phase condenses on the diesel and ammonium sulfate particles. This (aging) allows the hydrophobic diesel particles acquire water and activate alongside the already hydrophilic ammonium sulfate thus increasing the activation ratio of UV experiment to about 0.65- 0.85. For the dark experiments (triangles), only about 10% of the total particles became CCN at the end the experiment. For the dark experiments (filled triangle), the activation ratio increases over time. The reason for the increase in activation ratio observed remains unclear but could be due to the activation of ammonium sulfate seed particle or an increase in particle diameter due to the coagulation of ammonium sulfate and diesel exhaust particles (larger particle activates readily than smaller particles).

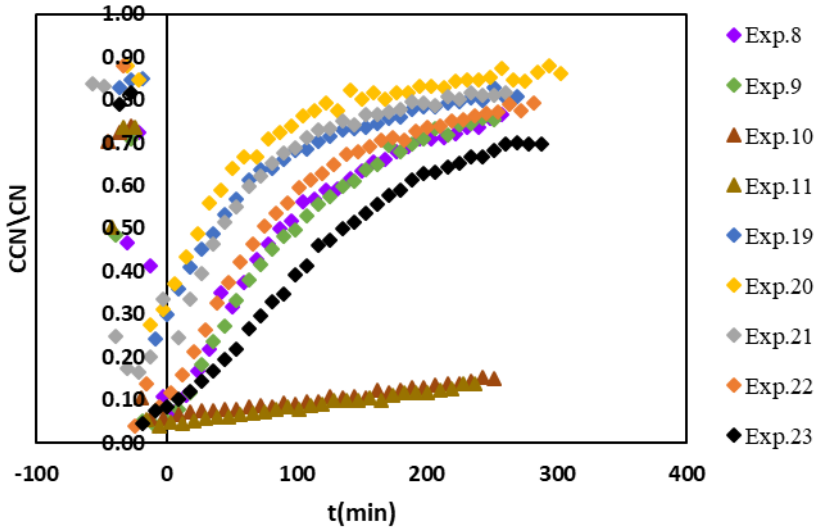

Figure 31. Activation Ratio of diesel exhaust+ ammonium sulfate seed particle experiments under UV radiation (diamonds) and dark (triangle) conditions.

5.4 Diesel Exhaust + α-pinene + Ammonium Sulfate Seed Particle Experiments

The list of diesel exhaust + α-pinene + ammonium sulfate seed particle experiments conducted, and their experimental conditions are shown in Table 5. A total of three runs were performed under UV conditions. The initial mass and number (ammonium sulfate seed and diesel exhaust particles) concentration of the particle injected into the chamber are in the range of 12-17×10^4 cm^{-3} and 66- 161 μgm^{-3} respectively. The mass fractions of ammonium sulfate seed particles in the initial mass ranges from 0.2 to 0.35. 39ppbv of α-pinene was volatilized and flushed into the chamber with particle free air. The temperature in the chamber was observed to be within 23-30°C. As shown in Table 5, the mass of the diesel exhaust particle increased by 23 - 62% due to the contributions of α-pinene and diesel exhaust vapor. The SS setting of the CCN counter changed from (0.88 to 0.597%), and (0.88 to 0.598%) after 63 and 34 minutes of reaction for Exp.25 and 26 respectively.

Table 5. Summary of Diesel Exhaust Particle with Ammonium Sulfate and Alpha Pinene Experiments and the Experimental Conditions.

Experiment No.	UV/Dark	Initial M ($\mu g/m^3$)	Initial N ($\#/cm^3$)	ΔM%	SMPS Particle Size Range (µm)	Alpha Pinene Conc. (ppbv)	$(NH_4)_2SO_4$ Mass Fraction	Temperature (^0C)	CCN Counter Supersaturation SS (%)
24	UV	161	24×10^4	42	14-685	39	0.20	23-30	0.626
25	UV	66	12×10^4	23	14-685	39	0.30	23-30	0.88, 0.597
26	UV	134	17×10^4	65	14-685	39	0..35	23-30	0.88, 0.598

5.4.1 Normalized Mass of Diesel Exhaust + α-pinene + Ammonium Sulfate Seed Particle Experiments

The normalized mass of diesel exhaust aged with ammonium sulfate and α-pinene is shown in Figure 32. The mass of Exp.25 (blue triangle) decreased initially by 10% and increased afterward. The normalized mass in Figure 32 increased over the time of the reaction. At the end of the experiment, the mass of the particles increased by factors of 1.1 to 1.6 (Figure 32) when compared to their initial mass. As shown in Table 5, changing the mass fraction of ammonium sulfate in initial particle mass does not seem to have an effect on ΔM%. Comparing the normalized mass in Figure 32 (mass increased by a factor of 1.1-1.6) to that in Figure 28 (Exp. 8,9,22 and 23. mass increased by a factor of 1.1-1.2), we observed that the addition of 39pbbv of α-pinene to the mixture of diesel exhaust and ammonium sulfate seed increased particle mass by 60% when compared to diesel exhaust +ammonium sulfate experiments (Figure 28).

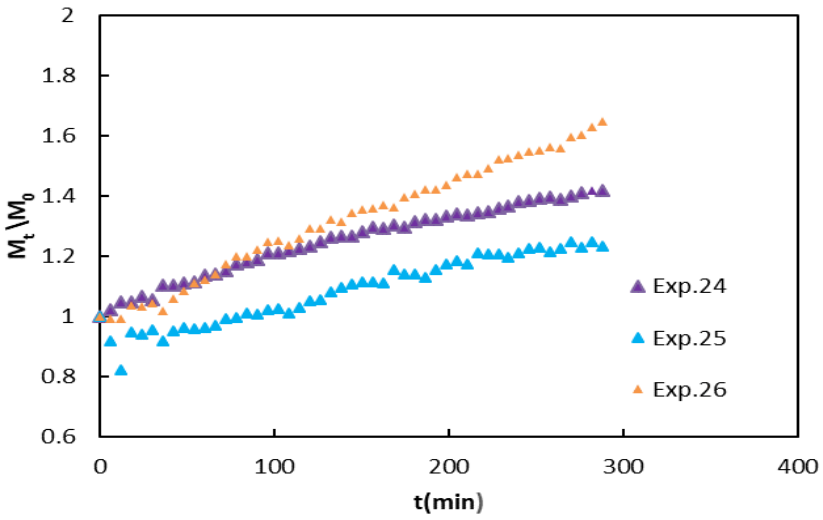

Figure 32. Normalized mass of diesel exhaust + α-pinene + ammonium sulfate seed particle experiments.

5.4.2 Kappa Value in Diesel Exhaust + α-pinene + Ammonium Sulfate Seed Particle Experiments

Kappa values for diesel exhaust particles aged in the presence of ammonium sulfate particle, α-pinene (39ppbv) and UV radiation are shown in Figure 33. Kappa values prior to time zero, when only ammonium sulfate particles were in the reactor were observed to be about 0.66 due to the to the activation of soluble ammonium sulfate particles. As the diesel exhaust particles were injected into the chamber, the kappa dropped to ~ 0.01 in all the experiments. As stated in section 5.3.2, the decrease in κ_{CCN} to ~0.01 (after diesel exhaust injection) does not mean that the ammonium sulfate particles stopped activating but is because of a single kappa value being calculated for a mixture of two distinct particle population. Afterwards, κ_{CCN} increased due to the photochemical oxidation of diesel exhaust and α-pinene and the activation of ammonium sulfate seed particles. The addition of 39ppbv of α-pinene had no discernible effect on kappa value since kappa values (0.1-0.2) observed after 250 minutes of aging are within the range of κ_{CCN} (0.03-0.3) shown in Figure 29.

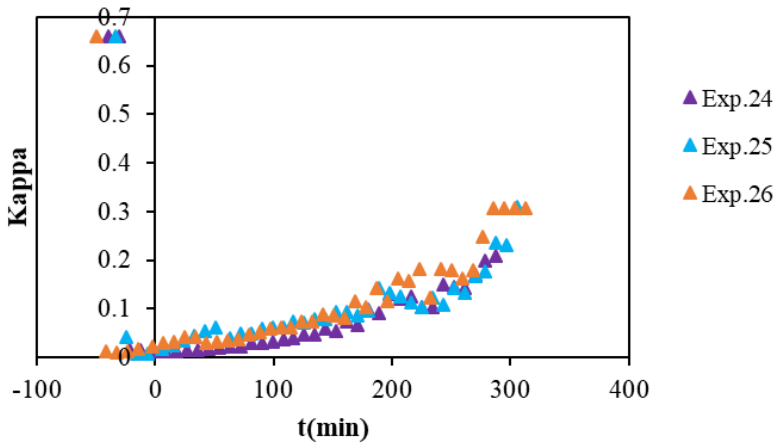

Figure 33. Kappa values of diesel exhaust + α-pinene + ammonium sulfate seed particle experiments.

5.4.3 Critical Diameter in Diesel Exhaust + α-pinene + Ammonium Sulfate Seed Particle Experiments

The critical diameter of the mixture containing diesel exhaust, α-pinene, and ammonium sulfate seed particle is shown in Figure 34. Before introducing diesel exhaust into the chamber, the critical diameter was observed to be in the range of 30-35nm due to the activation of soluble ammonium sulfate particles. When diesel exhaust was introduced into the chamber, the critical diameter increased to about 90-150nm (see Figure 34 at time zero). The critical diameter for all three experiments was observed to decrease with reaction time due to photochemical aging. However, for Exp 25 and Exp 26 there was a change in SS of the CCN counter during the experiment (a SS decrease occurred after 63 minutes for Exp.25 and 34 minutes for Exp.26). The change in SS (see Table 5) increased the Dpc to 93nm and 106nm for Exp 25 and 26 (see Figure 34) respectively. After the increase in D_{pc} due to SS change, D_{pc} continued to decrease with reaction time for both experiments due to the photochemical oxidation of α-pinene, diesel exhaust and the activation of ammonium sulfate seed particles. After 300 minutes of aging, particles of

diameter ranging from 50nm to 60nm could activate into cloud droplets. There is no discernible effect of alpha-pinene on D_{pc} since the critical diameter for the experiments in Figure 34 (60-70nm) is comparable to critical diameter for the experiments in Figure 30 (50-100nm).

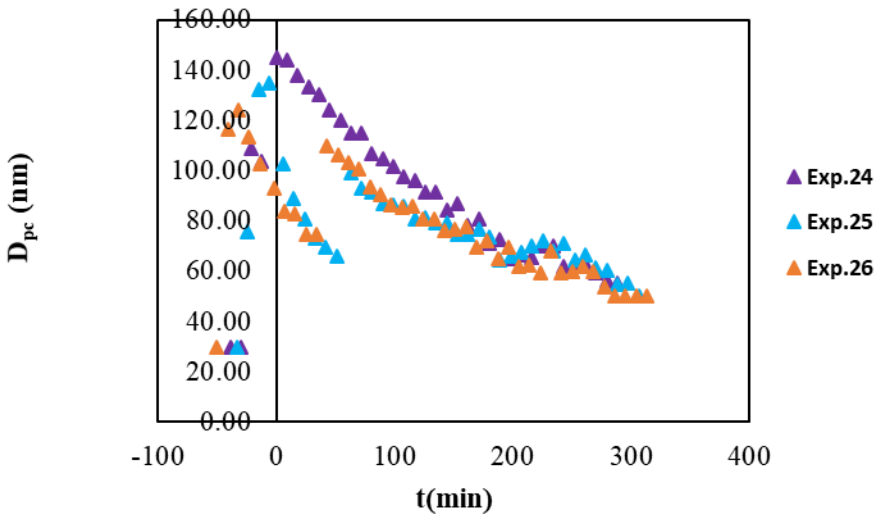

Figure 34. Critical diameter of diesel exhaust + α-pinene + ammonium sulfate seed particle experiments.

5.4.4 Activation Ratio in Diesel Exhaust + α-pinene + Ammonium Sulfate Seed Particle Experiments

Figure 35 presents the CCN activation of the diesel exhaust aged in the presence of α-pinene, ammonium sulfate seed particle, and UV radiation. Activation ratio for all the experiments were initially (before time zero) about 0.95-0.98 due to the activation of ammonium sulfate particles. When diesel exhaust was injected into the chamber, the activation ratio decreased to about 0.13. After diesel exhaust injection, the activation ratio for all three experiments was observed to increase over time due to the condensation of more soluble products on the particles and increase in particle diameter due to the condensation. As with the critical diameter results,

the change in SS of the CCN counter caused a sudden shift in the activation ratio for Exp 25 and Exp 26. The change in SS decreased the activation ratio to 0.32 and 0.47 for experiments 25 and 26 respectively. After the decreased in activation ratio due to the change in SS, the activation ratio was observed to continue to increase with reaction time as it had been doing previously due to the condensation of more soluble SOA on the particle and increase in particle diameter due to condensation. After 300 minutes of aging, 80-85 %(Exp, 25, 26 and 27) of the particles were activated.

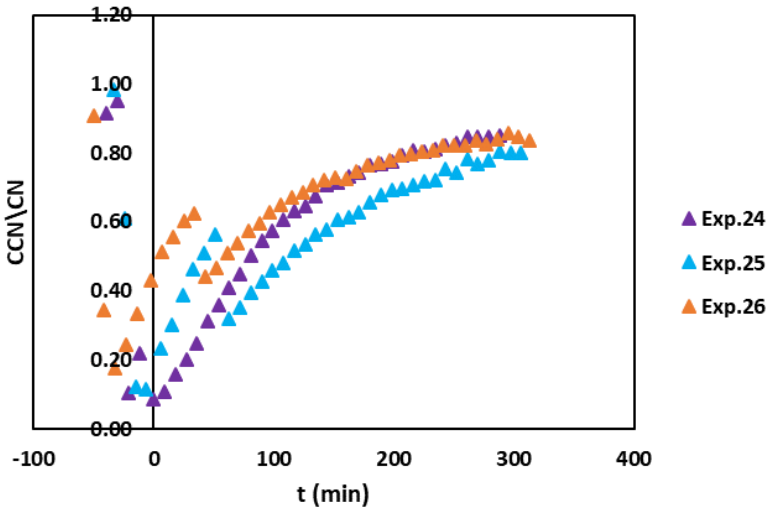

Figure 35. Activation ratio of diesel exhaust + α-pinene + ammonium sulfate seed particle Experiments.

CHAPTER VI

CONCLUSIONS AND RECOMMENDATIONS

6.1 Result Summary and Conclusions

The particle growth (SOA formation) and CCN activity of aging diesel exhaust particles generated by an idling (100rpm) V2403 Kubota diesel engine were studied in the University of North Dakota atmospheric aerosol chamber. The time-dependent changes in size distribution, number concentration, and activation were monitored with the primary focus on quantifying the SOA formation and CCN activity of diesel exhaust particles aged in the presence of one or more of the following: gas-phase diesel exhaust, UV- radiation, α-pinene, and ammonium sulfate seed particles.

The time-dependent particle size distribution and number concentration measured by the SMPS were converted to total mass (assuming particle density of $1 g/cm^3$). The total particle mass was corrected for particle-wall loss and normalized by the initial amount of diesel soot to compare SOA formation results of the different experiments conducted. To quantify the water uptake capability of the aging diesel exhaust particle, size-dependent CCN concentration measured by a CCN counter was aligned with size distribution data from an SMPS. The changes in critical diameter of the particles determined from Scanning Mobility CCN Analysis (SMCA) program developed by Moore et al. (2010), was used to estimate the kappa value of the particles as a function of reaction time.

Fresh soot showed no CCN activation. Also, no significant changes in CCN activation and SOA formation were observed for all the experiments performed under dark condition. The low kappa ($\kappa_{CCN} \sim 0$), low activation ratio (<1%) and high critical diameter observed for dark experiments confirms that fresh soot is hydrophobic and unable to activate into cloud droplets. The aging of the diesel exhaust in the presence of UV-radiation resulted in a significant increase in wall-loss corrected mass and CCN activation of the particles. While the critical diameter for activation was observed to decrease with reaction time, particle mass, kappa value, and activation ratio increase with reaction time. These results suggest transforming of soot particles into slightly hygroscopic and CCN active particles due to condensation of more water-soluble products on the particle, through changes in both chemical properties and particle size. The results also underscore the importance of sunlight in transforming soot particles.

SOA formation from and CCN activation of diesel exhaust were further enhanced with the addition of 39ppbv α-pinene (diesel exhaust + α-pinene experiments). The diesel exhaust particle mass, kappa values, and activation ratio further increased by 21%, 88%, and 7%, respectively, compared to the diesel exhaust experiments. These changes are due to the following: extra particle mass from condensing semi-volatile products formed from the photooxidation reactions of α-pinene, additional partitioning to the particle phase of semi-volatile products from diesel exhaust photooxidation, and the SOA formation from the photochemical reactions between diesel exhaust components and α -pinene. (Lee et al., 2004). Also, with the addition of α-pinene, the diameter required for activation (critical diameter) was significantly reduced after 200 minutes of reaction compared to the diesel exhaust experiments. The total SOA (diesel exhaust+

α-pinene) computed for this study was consistent with the SOA yield obtained by Lee et al., (2004).

Diesel exhaust particles were mixed with various amounts of ammonium sulfate seed particles to investigate how coagulation between diesel and ammonium sulfate particles impacts both CCN activity of hydrophobic diesel particle, and diesel particle mass growth. In the mixed diesel-ammonium sulfate experiments the mass of diesel particles decreased by a factor of 0.9-0.8 under dark condition. By exposing the mixture of diesel exhaust and ammonium sulfate to UV radiation, diesel exhaust particle mass increased by a factor of 1.1-1.2. κ_{CCN} was found to range from 0.02-0.3 after 200 minutes for UV experiments and remained approximately zero for dark experiments. Particle growth under UV radiation was higher for diesel exhaust alone than for the mixture of diesel exhaust and ammonium sulfate seed particles. The increase in activation ratio and kappa value and decrease in critical diameter with time for UV experiments were found to be correlated with the ammonium sulfate fraction in the mass of the particle. The experiments containing a higher mass fraction of ammonium sulfate showed a larger increase in kappa value and activation ratio. Also, the decline in critical diameter was more pronounced for the experiments with the higher fraction of ammonium sulfate mass. These results suggest that the photochemical oxidation of diesel exhaust in an environment containing ammonium sulfate particle make them hydrophilic enough to activate along with already hydrophilic ammonium sulfate particles.

The addition of 39ppbv α-pinene to the mixture of diesel exhaust and ammonium seed particles (diesel exhaust + α-pinene + ammonium sulfate seed particle experiments) enhances SOA formation. The mass of diesel exhaust particle increases by a factor of 1.1-1.6 after about

300 minutes of UV exposure. This increased mass represents a change in mass of +60%, +14%, and -6% when compared to diesel exhaust +ammonium seed particles, diesel exhaust, and diesel + α-pinene experiments, respectively. The addition of 39 ppbv of α-pinene had no discernible effect on kappa value (0.1-0.2), critical diameter (60-70nm), and activation ratio (0.75-0.8) with values comparable to the kappa (κCCN, 0.03-0.3), critical diameter (50-100nm) and activation ratio (0.65-0.85) observed in diesel exhaust + ammoniums sulfate seed particle experiments.

Results from this study indicate that the aging of diesel exhaust particles in the presence of gas-phase diesel exhaust, UV-radiation, α-pinene, and ammonium sulfate particle changes their chemical and physical properties in a way that is consistent with mechanisms such as condensation of semi-volatile compounds on the diesel particles, photochemical reaction in the particle phase, coagulation between the diesel particles, and coagulation with ammonium sulfate particles. This study has demonstrated that the size and CCN activity of diesel exhaust particles increases during aging. Also, it is expected that the aging of soot particles reduces their atmospheric lifetime because aged diesel particles can more easily be removed from the atmosphere by wet scavenging (when they are incorporated into existing cloud) and rainout (when they act as CCN). We have demonstrated that anthropogenic emission of diesel exhaust may contribute to SOA formation and that the resulting particle mass may be on the order of 1.0 to 1.4 higher than the mass of diesel particulate initially emitted into the atmosphere.

The results of UV experiments performed in this study emphasizes the importance of sunlight in initiating photochemical reactions that increase the CCN activity and SOA formation of diesel exhaust particles. Our result showed that CCN activity and SOA formation increased significantly under UV radiation. Since the lifetime of diesel particles in the atmosphere depends

on their CCN activity, our result indicates that the atmospheric lifetime of diesel particle may be longer in the winter than in the summer.

6.2 Recommendations and Future Work

In this thesis, we assumed that vapor deposition to the chamber walls was negligible. In the future, vapor deposition rates in the chamber should be studied, and the results incorporated to determine how vapor wall loss has affected the SOA formation aging of diesel exhaust particles.

Future work could also include studying the effect of temperature on gas-to - particle partitioning and CCN activity of aging diesel exhaust particles. Multiple runs could be conducted at different temperature. Also, for some runs, temperature in the chamber could be changed at different time during the reaction.

The use of gas chromatography to determine concentrations of gas-phase SOA precursors and photochemical oxidation products of aging diesel particles is recommended. Also, the changes in optical properties and morphology of aging diesel exhaust particle need to be investigated along with CCN activity for accurate characterization of the health and climate effects of diesel exhaust particles.

Additional experiments could also be done to study the atmospheric aging of diesel soot particles in the presence of other gas-phase SOA precursors.

APPENDIX

APPENDIX A

EXPERIMENTS AND THEIR EXPERIMENTAL CONDITIONS

EXPERIMENTS AND THEIR EXPERIMENTAL CONDITIONS

Experiment Number	Experiment	Date	UV/Dark	Initial M(μg/m³)	Initial N(#/cm³)	ΔM%	SMPS	Alpha Pinene Conc.(ppbv)	$(NH_4)_2SO_4$ Mass Fraction	Temperature (°C)	CCN Counter Supersaturation SS (%)
1	Diesel Exhaust Particle (DEP)	12.09.2016	UV	29	4.6×10^4	-2	8-352	No	No	23-32	0.16
2	DEP	12.12.2016	UV	74	11×10^4	37	8-352	No	No	23-32	0.6
3	DEP	12.14.2016	UV	34	5.4×10^4	12	8-352	No	No	23-32	0.74
4	DEP	12.16.206	Dark	62	9.0×10^4	-34	8-352	No	No	23-32	0.74
5	DEP	12.19.2016	Dark	74	9.3×10^4	-27	8-352	No	No	23-32	0.88
6	DEP	12.30.2016	UV	78	12×10^4	39	8-352	No	No	23-32	0.88
16	DEP	06.16.2017	UV	120	23×10^4	6	8-352	No	No	Reduced from 28°C to 20°C after 2 hours	0.88 and 0.6
17	DEP	07.12.2017	UV	188	15×10^4	9	8-352	No	No	25-28	No CCN
18	DEP	07.14.2017	UV	78	14×10^4	23	8-352	No	No	25-30	No CCN
12	DEP+α-Pinene	01.30.2017	UV	97	16×10^4	70	8-352	39	No	23-32	0.88
13	DEP+α-Pinene	02.07.2017	UV	107	15×10^4	45	8-352	39	No	23-32	0.88
14	DEP+α-Pinene	02.09.2017	UV	79	14×10^4	52	8-352	39	No	23-32	0.88
15	DEP+α-Pinene	03.20.2017	UV	68	7.6×10^4	72	8-352	39	No	23-32	No CCN
7	DEP+$(NH_4)_2SO_4$	01.04.2017	UV	25	3.7×10^4	11	8.-352	No	0.73	23-32	No CCN
8	DEP+$(NH_4)_2SO_4$	01.06.2017	UV	216	174×10^4	27	8-352	No	0.69	23-32	0.88
9	DEP+$(NH_4)_2SO_4$	01.09.2017	UV	129	13×10^4	34	8-352	No	0.49	23-32	0.88
10	DEP+$(NH_4)_2SO_4$	01.13.2017	Dark	211	13×10^4	-28	8-352	No	0.68	23-32	0.88
11	DEP+$(NH_4)_2SO_4$	01.17.2017	Dark	182	18×10^4	-23	8-352	No	0.61	23-32	0.88
19	DEP+$(NH_4)_2SO_4$	07.18.2017	UV	162	15×10^4	72	14-685	No	0.83	25-30	0.88
20	DEP+$(NH_4)_2SO_4$	07.20.2017	UV	105	9.6×10^4	93	14-685	No	0.75	25-30	0.88
21	DEP+$(NH_4)_2SO_4$	07.24.2017	UV	215	19×10^4	87	14-685	No	0.36	25-30	0.88
22	DEP+$(NH_4)_2SO_4$	07.26.2017	UV	174	24×10^4	22	14-685	No	0.28	25-30	0.88 and 0.639
23	DEP+$(NH_4)_2SO_4$	07.28.2017	UV	161	27×10^4	33	14-685	No	0.35	25-30	0.586
24	DEP+$(NH_4)_2SO_4$+α-Pinene	08.01.2017	UV	161	24×10^4	42	14-685	39	0.2	23-30°C	0.88 and 0.626
25	DEP+$(NH_4)_2SO_4$+α-Pinene	08.03.2017	UV	66	12×10^4	26	14-685	39	0.3	23-30°C	0.88 and 0.597
26	DEP+$(NH_4)_2SO_4$+α-Pinene	08.09.2017	UV	134	17×10^4	82	14-685	39	0..35	23-30°C	0.88 and 0.598

REFERENCES

Albrecht, B. (1989). Aerosols, Cloud Microphysics, and Fractional Cloudiness. *Science, 245*(4923), 1227–1230.

Baek, B., Aneja, V., and Tong, Q. (2004). Chemical coupling between ammonia, acid gases, and fine particles. *Environmental Pollution, 129*(1), 89–98.

Bassett, M., and Seinfeld, J. (1984). Atmospheric equilibrium model of sulfate and nitrate aerosols-II. Particle size analysis. *Atmospheric Environment (1967), 18*(6), 1163–1170

Bernstein, J., Alexis, N., Barnes, C., Bernstein, I., Nel, A., Peden, D., . . . Williams, P. (2004). Health effects of air pollution. *Environmental Progress114*(0091–6749, 1116–1123.

BUWAL, Feinstaub macht krank, BUWAL (Bundesamt f¨ur Umwelt, Wald und Landschaft, ed.), Bern, (2005) http://www.bafu.admin.ch/luft/,

Chameides, W., and Bergin, M. (2002). Climate change. Soot takes center stage. *Science (New York, N.Y.), 297*(5590), 2214–2215

Chin, M., Kahn, R. A., Remer, L. A., Yu, H. B., Rind, D., Feingold, G., … DeCola, P. (2009). Atmospheric aerosol properties and climate impacts. *Atmospheric Aerosol Properties and Climate Impact*.

Cooke, W., and Wilson, J. (1996). A global black carbon aerosol model. *Journal of Geophysical Research: Atmospheres, 101*(D14), 19395–19409.

Curry, J.A.; Webster, P. (1999). *Thermodynamics of Atmospheres and Oceans* (1 ed.). New York: Academic Press.

DeCarlo, P., Slowik, J., Worsnop, D., Davidovits, P., and Jimenez, J. (2005). Erratum: Particle morphology and density characterization by combined mobility and aerodynamic diameter measurements. Part 1: Theory (Aerosol Science and Technology 38, 10 (1185-1205)). *Aerosol Science and Technology*.

Dusek, U., Reischl, G., and Hitzenberger, R. (2006). CCN activation of pure and coated carbon black particles. *Environmental Science and Technology*, *40*(4), 1223–1230.

Fan, J., Zhang, R., Tao, W.-K., and Mohr, K. (2008). Effects of aerosol optical properties on deep convective clouds and radiative forcing. *Journal of Geophysical Research-Atmospheres*, *113*, *D0820*(D8).

Fassi-Fihri, A., Suhre, K., and Rosset, R. (1997). Internal and external mixing in atmospheric aerosols by coagulation: Impact on the optical and hygroscopic properties of the sulfate-soot system. Atmospheric Environment, 31(10), 1393–1402

Finlayson-Pitts, B., and Pitts, J. (2000). *Chemistry of the Upper and Lower Atmosphere: Theory, Experiments, and Applications.*

Forster, P., Ramaswamy, V., Artaxo, P., Berntsen, T., Betts, R., Fahey, D., . . . Dorland, R. (2007). Changes in Atmospheric Constituents and in Radiative Forcing. In: Climate Change 2007: The Physical Science Basis. In P. Forster, V. Ramaswamy, P. Artaxo, T. Berntsen, R. Betts, D. Fahey, . . . R. Dorland, *Contribution of Working Group I to the Fourth Assessment Report of the Intergovernmental Panel on Climate Change.*

Geron, C., Rasmussen, R., R. Arnts, R., and Guenther, A. (2000). A review and synthesis of monoterpene speciation from forests in the United States. *Atmospheric Environment*, 34(11), 1761–1781.

Guo, S., Hu, M., Lin, Y., Gomez-Hernandez, M., Zamora, M., Peng, J., . . . Zhang, R. (2016). OH-Initiated Oxidation of m-Xylene on Black Carbon Aging. *Environmental Science and Technology*, *50*(16), 8605–8612

Haywood, J., and Boucher, O. (2000). Estimates of the direct and indirect radiative forcing due to tropospheric aerosols: A review. *Reviews of Geophysics*.

Henning, S., Ziese, M., Kiselev, A., Saathoff, H., Möhler, O., Mentel, T., . . . Stratmann, F. (2012). Hygroscopic growth and droplet activation of soot particles: Uncoated, succinic or sulfuric acid coated. *Atmospheric Chemistry and Physics*, , *12*(10), 4525–4537

Hinds, W. (1999). *Aerosol technology: Properties, Behavior, and Measurement of Airborne Particles.*

Hings, S., Wrobel, W., Cross, E., Worsnop, D., Davidovits, P., and Onasch, T. (2008). CCN activation experiments with adipic acid: effect of particle phase and adipic acid coatings on soluble and insoluble particles. *Atmospheric Chemistry and Physics Discussions*. , *8*, 4439–4482.

IPCC. (2007). Climate Change 2007: The Physical Science Basis. Contribution of Working Group I to the Fourth Assessment Report of the Intergovernmental Panel on Climate Change. (S. Solomon, D. Qin, M. Manning, Z. Chen, M. Marquis, K. B. Averyt, H. L. Miller, Eds.), IPCC, 2007: Climate Change 2007: The Physical Science Basis. Contribution of Working Group, I to the Fourth Assessment Report of the Intergovernmental Panel on Climate Change (p. 35). Cambridge, UK: Cambridge University Press

International Agency for Research on Cancer(IARC). (2012). Diesel engine exhaust carcino genic. *World Health Organization*.

Jacobson, M., Hansson, H., Noone, K., and Charlson, R. (2000). Organic atmospheric aerosols: Review and state of the science. *Reviews of Geophysics*, *38*(2), 267–294.

Jacobson, M. Z. (2001). Strong radiative heating due to the mixing state of black carbon in atmospheric aerosols. *Nature*, *409*(6821), 695–697

Katsouyanni, K., Touloumi, G., Samoli, E., Gryparis, A., Le Tertre, A., Monopolis, Y., . . . Schwartz, J. (2001). Confounding and Effect Modification in the Short-Term Effects of Ambient Particles on Total Mortality: Results from 29 European Cities within the APHEA2 Project. *Epidemiology*, *12*(5), 521–531

Khalizov, A. F., Zhang, R., Zhang, D., Xue, H., Pagels, J., & McMurry, P. H. (2009). Formation of highly hygroscopic soot aerosols upon internal mixing with sulfuric acid vapor. *Journal of Geophysical Research Atmospheres*, *114*(5).

Khalizov, A., Lin, Y., Qiu, C., Guo, S., Collins, D., and Zhang, R. (2013). Role of OH-initiated oxidation of isoprene in aging of combustion soot. *Environmental Science and Technology*, *47*(5), 2254–2263.

Kittelson, D. (1998). Engines and nanoparticles: A review. *Journal of Aerosol Science*, 29 575–88

Koelmans, A., Jonker, M., Cornelissen, G., Bucheli, T., Van Noort, P., and Gustafsson, Ö. (2006). Black carbon: The reverse of its dark side. *Chemosphere*.

Köhler, H., (1936) The nucleus in and the growth of hygroscopic droplets, ¨ *T. Faraday Soc.*, 32(2), 1152–1161.

Kotzick, R., and Niessner, R. (1999). The effects of aging processes on critical supersaturation ratios of ultrafine carbon aerosols. *Atmospheric Environment*, *33*(17), 2669–2677

Lambe, A., Ahern, A., Wright, J., Croasdale, D., Davidovits, P., and Onasch, T. (2015). Oxidative aging and cloud condensation nuclei activation of laboratory combustion soot. *Journal of Aerosol Science*, *79*, 31–39.

Lary, D., Shallcross, D., and Toumi, R. (1999). Carbonaceous aerosols and their potential role in atmospheric chemistry. *Journal of Geophysical Research-Atmospheres*.

Lee, S., Jang, M., and Kamens, R. M. (2004). SOA formation from the photooxidation of α-pinene in the presence of freshly emitted diesel soot exhaust. *Atmospheric Environment*, *38*(16), 2597–2605.

Lei, W., Zhang, R., Tie, X., & Hess, P. (2004). Chemical characterization of ozone formation in the Houston-Galveston area: A chemical transport model study. *Journal of Geophysical Research D: Atmospheres*.

Leskinen, A., Jokiniemi, J., and Lehtinen, K. (2007). Transformation of diesel engine exhaust in an environmental chamber. *Atmospheric Environment*, *41*(39), 8865–8873.

Li, G., Zhang, R., Fan, J., and Tie, X. (2005). Impacts of black carbon aerosol on photolysis and ozone. *Journal of Geophysical Research Atmospheres*, *110*(23), 1–10

Liousse, C., Penner, J., Chuang, Z., Walton, J., Eddleman, H., and Cachier, H. (1996). A global three-dimensional model study of carbonaceous aerosols. *Journal of Geophysical Research*, *101*(D14), 19411–19432.

Lohmann, U., and Feichter, J. (2004). Global indirect aerosol effects: a review. *Atmospheric Chemistry and Physics Discussions*, *4*(6), 7561–7614.

McCormick, R., and Ludwig, J. (1967). Climate modification by atmospheric aerosols. *Science*, *156*(780), 1358–1359.

McFiggans, G., Artaxo, P., Baltensperger, U., Coe, H., Facchini, M., Feingold, G., . . . Weingartner, E. (2006). The effect of physical and chemical aerosol properties on warm cloud droplet activation. *Atmospheric Chemistry and Physics Discussions*, *5*(5), 8507–8646

Middlebrook, A., Murphy, D., and Thomson, D. (1998). Observations of organic material in individual marine particles at Cape Grim during the First Aerosol Characterization Experiment (ACE 1). *Journal of Geophysical Research: Atmospheres 103*(D13), 16475–16483.

Moore, R., Nenes, A., and Medina, J. (2010). Scanning mobility CCN analysis-A method for fast measurements of size-resolved CCN distributions and activation kinetics. *Aerosol Science and Technology*.*44*(10), 861–871.

Moore, R. H., and A. Nene's (2009), Scanning flow CCN analysis – a method for fast measurements of CCN spectra, Aer. Sci. Tech., 43, 1192-1207,

Nakao, S., Shrivastava, M., Nguyen, A., Jung, H., & Cocker, D. (2011). Interpretation of secondary organic aerosol formation from diesel exhaust photooxidation in an environmental chamber. *Aerosol Science and Technology*, *45*(8), 964–972.

Pathak, R., Wu, W., and Wang, T. (2009). Summertime PM_{2.5} ionic species in four major cities of China: nitrate formation in an ammonia-deficient atmosphere. *Atmospheric Chemistry and Physics*, *9*(5), 1711–1722.

Penner, J., Chuang, C., & Grant, K. (1998). Climate forcing by carbonaceous and sulfate aerosols. *Climate Dynamics*,*14*(12), 839–851.

Penner, J. E., Eddleman, H., & Novakov, T. (1993). Towards the Development of a Global Inventory for Black Carbon Emissions. *Atmos. Environ. Part a-General Topics*, *27*(8), 1277–1295.

Petters, M. D., and Kreidenwies, S. M. (2007). A single parameter representation of hygroscopic growth and cloud condensation nucleus activity. *Atmos. Chem. Phys.*, 1961–1971.

Pope, C., Burnett, R., Thurston, G., Thun, M., Calle, E., Krewski, D., and Godleski, J. (2004). Cardiovascular Mortality and Long-Term Exposure to Particulate Air Pollution: Epidemiological Evidence of General Pathophysiological Pathways of Disease. *Circulation*, *109*(1), 71–77

Pope, C. A., & Dockery, D. W. (2006). Health effects of fine particulate air pollution: lines that connect. *J Air Waste Manag Assoc*, *56*(6), 709–742.

Pope, C., Ezzati, M., and Dockery, D. (2009). Fine-Particulate Air Pollution and Life Expectancy in the United States. *New England Journal of Medicine*, *360*(4), 376–386.

Pöschl, U. (2005). Atmospheric aerosols: Composition, transformation, climate and health effects. *Angewandte Chemie - International Edition*.

Pruppacher, H., and Klett, J. (1978). Microstructure of Atmospheric Clouds and Precipitation. In H. Pruppacher, & J. Klett, *Microphysics of Clouds and Precipitation.*

Pruppacher, H., and Klett, J. (2004). Growth of Cloud Drops by Collision, Coalescence and Breakup. *Microphysics of Clouds and Precipitation*.

Qiu, C., Khalizov, A., and Zhang, R. (2012). Soot aging from OH-initiated oxidation of toluene. *Environmental Science and Technology*, *46*(17), 9464–9472

Raes, F., Dingenen, R., Elisabetta, V., Wilson, J., Putaud, J., Seinfeld, J., and Adams, P. (2002). Chapter 18 Formation and cycling of aerosols in the global troposphere. *Developments in Environmental Science*, *1*(C), 519–563.

Roberts, G. C. and A. Nenes (2005), A continuous-flow stream-wise thermal-gradient CCN chamber for atmospheric measurements, Aer. Sci. Tech., 39, 206-221.

Rose, D., Wehner, B., Ketzel, M., Engler, C., Voigtländer, J., Tuch, T., and Wiedensohler, A. (2006). Atmospheric number size distributions of soot particles and estimation of emission factors. *Atmospheric Chemistry and Physics*, *5*, 10125–10154.

Salvi, S., and Holgate, S. T. (1999). Mechanisms of particulate matter toxicity. *Clinical and Experimental Allergy*

Saxena, P., Hildemann, L., McMurry, P., and Seinfeld, J. (1995). Organics alter hygroscopic behavior of atmospheric particles. *Journal of GeophysicalResearch: Atmospheres*. *100*(D9), 18755–18770

Seinfeld, J., & Pandis, S. (1998). *Atmospheric chemistry and physics : from air pollution to climate change.*

Seinfeld, J., & Pandis, S. (2006). Atmospheric chemistry and physics: from air pollution to climate change. *Atmospheric chemistry and physics: from air pollution to climate change*.

Seol, K., Yabumoto, J., and Takeuchi, K. (2002). A differential mobility analyzer with adjustable column length for wide particle-size-range measurements. *Journal of Aerosol Science*, *33*(11), 1481–1492.

Stockwell, W., Kuhns, H., Etyemezian, V., Green, M., Chow, J., and Watson, J. (2003). The Treasure Valley secondary aerosol study II: Modeling of the formation of inorganic secondary aerosols and precursors for southwestern Idaho. *Atmospheric Environment*, *37*(4), 525–534.

Stokes, R. H. and Robinson, R. A., (1966) Interactions in aqueous nonelectrolyte solutions. I. Solute– solvent equilibria, J. Phys. Chem., 70(7), 2126–2130.

Sydbom, A. Blomberg, S. Parnia, N. Stenfors, T. Sandström, and S-E. Dahlén. (2001). Health effects of diesel exhaust emissions. *Health effects of diesel exhaust emissions*. *Eur. Respir. J.*, *17*(4), 733–746

Tritscher, T., Jurányi, Z., Martin, M., Chirico, R., Gysel, M., Heringa, M., . . . Baltensperger, U. (2011). Changes of hygroscopicity and morphology during ageing of diesel soot. *Environmental Research Letters*, *6*(3), 034026.

Twomey, S. (1977). The Influence of Pollution on the Shortwave Albedo of Clouds. *Journal of the Atmospheric Sciences*, 34(7), 1149–1152.

Twomey, S. (1974). Pollution and the Planetary Albedo. *Atmospheric Environment* , 8, 1251-1256.

Wang, Y., Fang, J., Attoui, M., Chadha, T. S., Wang, W. N., and Biswas, P. (2014). Application of Half Mini DMA for sub 2nm particle size distribution measurement in an electrospray and a flame aerosol reactor. *Journal of Aerosol Science*, *71*, 52–64 .

Warner, J. (1968). A Reduction in Rainfall Associated with Smoke from Sugar-Cane Fires—An Inadvertent Weather Modification? *Journal of Applied Meteorology*.

Weingartner, E., Burtscher, H., and Baltensperger, U. (1996). Hydration properties of Diesel soot particles. *J. Aerosol Sci, 27*, S695--S696.

Weingartner, E., Burtscher, H., and Baltensperger, U. (1997). Hygroscopic properties of carbon and diesel soot particles. *Atmospheric Environment*, 31(15), 2311–2327

Weitkamp, E., Sage, A., Pierce, J., Donahue, N., and Robinson, A. (2007). Organic aerosol formation from photochemical oxidation of diesel exhaust in a smog chamber. *Environmental Science and Technology*, *41*(20), 6969–6975.

Whitby, K., and Cantrell, B. (1976). Atmospheric aerosols- Characteristics and measurement. *International Conference on Environmental Sensing and Assessment, Las Vegas, Nev.*

Williams, J., de Reus, M., Krejci, R., Fischer, H., and Ström, J. (2002). Application of the variability-size relationship to atmospheric aerosol studies: estimating aerosol lifetimes and ages. *Atmospheric Chemistry and Physics Discussions*, *2*(1), 43–74

Winkler, P. (1973). The growth of atmospheric aerosol particles as a function of the relative humidity-II. An improved concept of mixed nuclei. *Journal of Aerosol Science*, *4*(5), 373–387

Wittbom, C., Eriksson, A., Rissler, J., Carlsson, J., Roldin, P., Nordin, E., . . . Svenningsson, B. (2014). Cloud droplet activity changes of soot aerosol upon smog chamber ageing. *Atmospheric Chemistry and Physics*, *14*(18), 9831–9854.

Zhang, R., Khalizov, A., Pagels, J., Zhang, D., Xue, H., and McMurry, P. (2008). Variability in morphology, hygroscopicity, and optical properties of soot aerosols during atmospheric processing. *Proceedings of the National Academy of Sciences*10291–10296.

Zuberi, B., Johnson, K., Aleks, G., Molina, L., Molina, M., and Laskin, A. (2005). Hydrophilic properties of aged soot. *Geophysical Research Letters*, *32*(1), 1–4.